UNIVERSITY OF AMSTERDAM

UvA-DARE (Digital Academic Repository)

Capturing the electromagnetic counterparts of binary neutron star mergers through low-latency gravitational wave triggers

Chu, Q.; Howell, E.J.; Rowlinson, A.; Gao, H.; Zhang, B.; Tingay, S.J.; Boër, M.; Wen, L.

DOI
10.1093/mnras/stw576

Publication date
2016

Document Version
Final published version

Published in
Monthly Notices of the Royal Astronomical Society

Link to publication

Citation for published version (APA):
Chu, Q., Howell, E. J., Rowlinson, A., Gao, H., Zhang, B., Tingay, S. J., Boër, M., & Wen, L. (2016). Capturing the electromagnetic counterparts of binary neutron star mergers through low-latency gravitational wave triggers. *Monthly Notices of the Royal Astronomical Society*, *459*(1), 121-139. https://doi.org/10.1093/mnras/stw576

General rights
It is not permitted to download or to forward/distribute the text or part of it without the consent of the author(s) and/or copyright holder(s), other than for strictly personal, individual use, unless the work is under an open content license (like Creative Commons).

Disclaimer/Complaints regulations
If you believe that digital publication of certain material infringes any of your rights or (privacy) interests, please let the Library know, stating your reasons. In case of a legitimate complaint, the Library will make the material inaccessible and/or remove it from the website. Please Ask the Library: https://uba.uva.nl/en/contact, or a letter to: Library of the University of Amsterdam, Secretariat, P.O. Box 19185, 1000 GD Amsterdam, The Netherlands. You will be contacted as soon as possible.

UvA-DARE is a service provided by the library of the University of Amsterdam (https://dare.uva.nl)

Download date:11 Oct 2026

Monthly Notices
of the
ROYAL ASTRONOMICAL SOCIETY

MNRAS **459,** 121–139 (2016)
Advance Access publication 2016 March 11

doi:10.1093/mnras/stw576

Capturing the electromagnetic counterparts of binary neutron star mergers through low-latency gravitational wave triggers

Q. Chu,[1⋆] E. J. Howell,[1⋆] A. Rowlinson,[2,3,4] H. Gao,[5] B. Zhang,[6] S. J. Tingay,[7,8] M. Boër[9] and L. Wen[1⋆]

[1]*School of Physics, University of Western Australia, Crawley, WA 6009, Australia*
[2]*CSIRO Astronomy and Space Science, Sydney, NSW 1710, Australia*
[3]*Anton Pannekoek Institute, University of Amsterdam, Postbus 94249, NL-1090 GE Amsterdam, the Netherlands*
[4]*The Netherlands Institute for Radio Astronomy (ASTRON), PO Box 2, NL-7990 AA Dwingeloo, the Netherlands*
[5]*Department of Astronomy, Beijing Normal University, Beijing 100875, China*
[6]*Department of Physics and Astronomy, University of Nevada, Las Vegas, NV 89154, USA*
[7]*International Centre for Radio Astronomy Research, Curtin University, Perth, WA 6845, Australia*
[8]*ARC Centre of Excellence for All-sky Astrophysics (CAASTRO), Australia*
[9]*CNRS – ARTEMIS, Boulevard de l'Observatoire, CS 34229, F-06304 Nice Cedex 04, France*

Accepted 2016 March 8. Received 2016 March 4; in original form 2015 September 21

ABSTRACT

We investigate the prospects for joint low-latency gravitational wave (GW) detection and prompt electromagnetic (EM) follow-up observations of coalescing binary neutron stars (BNSs). For BNS mergers associated with short duration gamma-ray bursts (SGRBs), we for the first time evaluate the feasibility of rapid EM follow-ups to capture the prompt emission, early engine activity, or reveal any potential by-products such as magnetars or fast radio bursts. To achieve our goal, we first simulate a population of coalescing BNSs using realistic distributions of source parameters and estimate the detectability and localization efficiency at different times before merger. We then use a selection of facilities with GW follow-up agreements in place, from low-frequency radio to high-energy γ-ray to assess the prospects of prompt follow-up. We quantify our assessment using observational SGRB flux data extrapolated to be within the horizon distances of the advanced GW interferometric detectors LIGO and Virgo and to the prompt phase immediately following the binary merger. Our results illustrate that while challenging, breakthrough multimessenger science is possible with EM follow-up facilities with fast responses and wide fields-of-view. We demonstrate that the opportunity to catch the prompt stage ($<$5 s) of SGRBs can be enhanced by speeding up the detection pipelines of both GW observatories and EM follow-up facilities. We further show that the addition of an Australian instrument to the optimal detector network could possibly improve the angular resolution by a factor of 2 and thereby contribute significantly to GW–EM multimessenger astronomy.

Key words: gravitational waves – methods: observational – binaries: close – gamma-ray burst: general – stars: neutron.

1 INTRODUCTION

The Laser Interferometer Gravitational-Wave Observatory (LIGO) detection of GW 150914 from the inspiral and merger of a pair of black holes has ignited a new era of astronomy (Abbott et al. 2016a). To fully exploit this new frontier it has been expected that triggered follow-ups by facilities operating outside the gravitational wave (GW) spectrum will become common place. During this new multimessenger era, prompt electromagnetic (EM) follow-ups from low-latency GW triggers can provide a pan-spectral pathway of understanding into the inner engines and underlying mechanisms behind a multitude of GW sources.

The Advanced LIGO (aLIGO; Aasi et al. 2015) detector launched its first science operations at sensitivities that would allow the detection of coalescing systems of binary neutron stars (BNSs) in the range of 40–80 Mpc;[1] aLIGO will be followed by Advanced

⋆E-mail: qi.chu@uwa.adu.au (QC); eric.howell@uwa.edu.au (EJH); linqing.wen@uwa.edu.au (LW)

[1] This range refers to the detectable range averaged over all sky locations and source orientations for BNS systems with individual masses of 1.4 $M_\odot$.

© 2016 The Authors
Published by Oxford University Press on behalf of the Royal Astronomical Society

Downloaded from https://academic.oup.com/mnras/article-abstract/459/1/121/2608842 by Universiteit van Amsterdam user on 03 July 2020

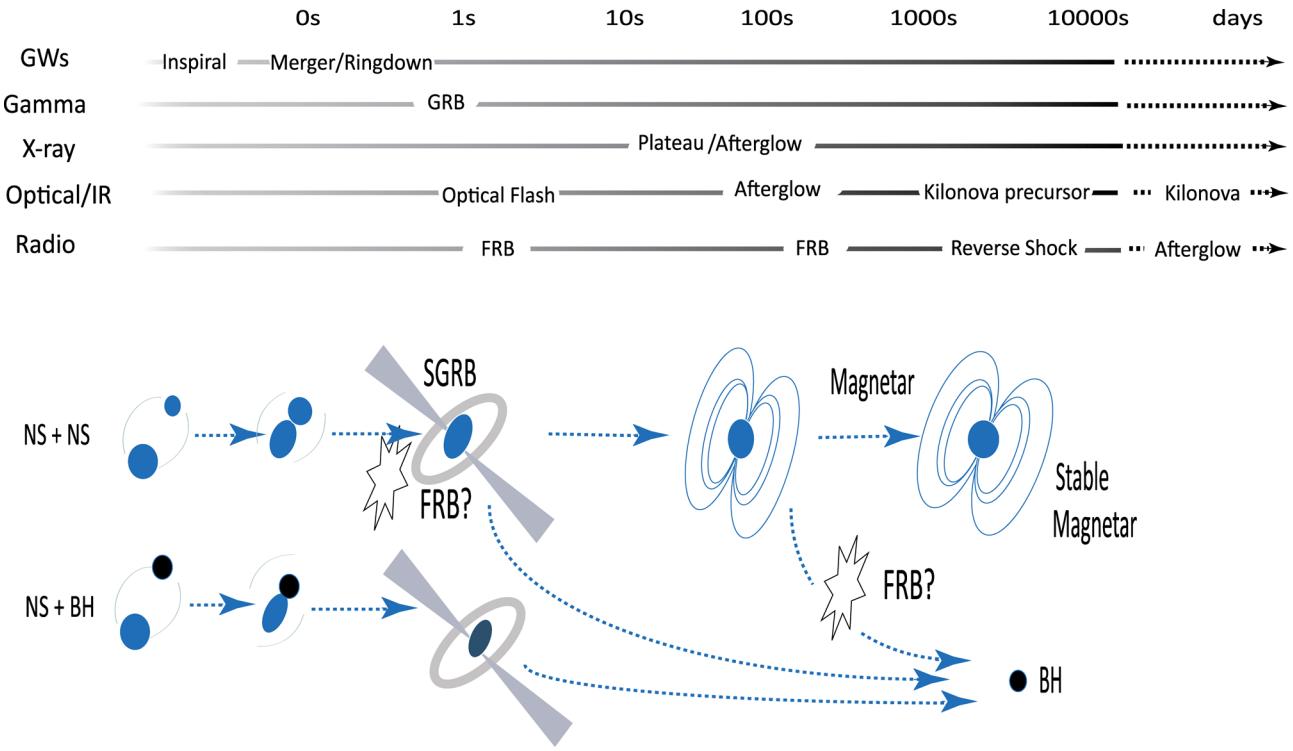

Figure 1. A cartoon illustrating some of the possible multimessenger pathways and end products of coalescing systems of NSs and BHs in different energy bands. We also show the approximate time-scales from GW merger. SGRBs are strongly linked with the merger of compact objects (Paczynski 1986; Eichler et al. 1989; Narayan, Paczynski & Piran 1992; Berger et al. 2005; Gehrels et al. 2005; Bloom et al. 2006; Rezzolla et al. 2011) and could be accompanied by an optical flash or a FRB (Totani 2013). If a stable or supramassive magnetar is formed, the long lived X-ray plateaus observed in many SGRBs could be the signature of direct dissipation of magnetar wind energy (Rowlinson et al. 2010b, 2013; Zhang 2013); the collapse of a merger product to a black hole could also produce an FRB (Falcke & Rezzolla 2014; Zhang 2014). At later times predictions for an optical/IR kilonova (Li & Paczyński 1998; Metzger et al. 2010; Barnes & Kasen 2013) have gained support though recent observations (Berger, Fong & Chornock 2013; Tanvir et al. 2013). For a relatively small opacity, a kilonova precursor may appear early enough which would benefit from the low-latency observations (Metzger et al. 2015).

Virgo (AdV; Acernese et al. 2015) later this year (2016). By 2019 aLIGO is expected to reach design sensitivity, with a BNS detection range of 200 Mpc. AdV is expected to reach this milestone by 2018 with BNS observations out to a distance of 130 Mpc (Acernese et al. 2015). Other second-generation detectors are also planned or undergoing construction. KAGRA, a Japanese instrument, is envisioned to begin operation in 2017 (Aso et al. 2013) and fulfil its baseline design around 2018–2019 (Somiya 2012). LIGO-India (Aasi et al. 2013) has obtained approval and is expected to be operational from 2020, reaching a design sensitivity at the same level as aLIGO no earlier than 2022 (Aasi et al. 2013).

Coalescing systems of BNSs are promising sources of GWs due to the fact that the inspiral phase is well modelled by the post-Newtonian (PN) approximation. The relatively low masses of BNS systems mean that these events will span most of the frequency band of aLIGO detectors. At design sensitivity, aLIGO is predicted to make 0.4–400 BNS detections per year according to current rate predictions (Abadie et al. 2010; Coward et al. 2012). The coalescence rate of binary systems comprising neutron stars and black holes (NS/BH) and binary black holes (BBH) are less confidently predicted due to a sparsity of observational data. Studies have predicted yearly detection rates of order 0.2–300 detections for NS/BH events and 0.4–1000 for BBH events (Abadie et al. 2010). For systems including at least one BH the detection of GW 150914 is important as it proved that BH birth kicks do not always break up the evolutionary formation channels for these sources (Abbott et al. 2016b).

Multimessenger astronomy is one of the highly prioritized research areas in the GW community (Howell et al. 2015). Complementary observations from EM, neutrino or high-energy particle facilities would not only improve the confidence of a GW detection, but also maximize the science return by providing a wealth of additional astrophysical information. A number of plausible EM emission mechanisms and end products that could be produced during the inspiral and merger phase of coalescing compact objects have been proposed. We summarize some of the popular scenarios in Fig. 1; predictions are highly uncertain as illustrated by the various pathways and end products and could involve combinations of BHs and/or magnetar formation or fast radio bursts (FRBs). The anticipated onset time, duration, and observable wavelengths shown suggest that transient EM emission could possibly occur within a few seconds after the binary merger (Centrella, Nissanke & Williams 2012; Metzger & Berger 2012). To catch these events, generating GW event triggers without delay (thus low-latency) and obtaining prompt EM follow-ups are crucial. Achieving joint GW–EM observations of these events could reveal the major processes and interactions at play during the binary merger process (see detailed discussion in Section 5).

A significant effort from both GW and EM astronomy community has been undertaken to achieve prompt GW-triggered EM

It is approximately 1/2.26 of the horizon distance – the range for optimally oriented and located sources.

Downloaded from https://academic.oup.com/mnras/article-abstract/459/1/121/2608842 by Universiteit van Amsterdam user on 03 July 2020

follow-up observations (Abadie et al. 2012; Shawhan 2012), though as yet, no joint GW–EM detections have been made. Recent developments in the areas of astronomical and computing technologies in the following three fronts will further improve the chance of catching EM transients during the binary coalescence.

(i) Advances in low-latency GW search pipelines that are capable of generating event triggers within minutes upon the arrival of a detectable signal.
(ii) Localizations are likely to improve as more GW detectors are constructed.
(iii) Development of wide-field EM telescopes capable of rapid response within tens of seconds and with fields of view (FoV) comparable to the error area of GW source sky direction (typically tens of square degrees for the aLIGO/AdV network).

The first point has been studied since the initial LIGO era and a number of low-latency GW trigger-generation pipelines have been proposed and tested (Buskulic et al. 2010; Abadie et al. 2012; Cannon et al. 2012; Hooper et al. 2012; Luan et al. 2012); the prospects of rapid alerts from GW events are discussed in Shawhan (2012).

The benefits of a larger network given in the second point have prompted studies of source localization by advanced networks by a number of authors (see the studies of Fairhurst 2011; Schutz 2011; Vitale & Zanolin 2011; Chu, Wen & Blair 2012; Aasi et al. 2013; Nissanke, Kasliwal & Georgieva 2013). Wen, Fan & Chen (2008), Fairhurst (2009), Wen & Chen (2010), Zanolin, Vitale & Makris (2010), Abadie et al. (2010), Nissanke et al. (2011), Klimenko et al. (2011) have investigated key aspects of source localization and estimation of localization accuracy. For low-latency detections, studies of the early localization of BNS sources when their GWs are detected tens of seconds before the merger can be found in Manzotti & Dietz (2012) and Cannon et al. (2012).

A recent study of the sky localization (Singer et al. 2014) for the early detector network expected in 2016–2017 indicate that the error in GW localization will be of order 200 deg^2. Methods of identifying GW sources from a large sky error regions will therefore have great importance and have been proposed by Nissanke et al. (2013), Fan, Messenger & Heng (2014), and Cowperthwaite & Berger (2015).

To combat the large error regions the range of wide-field EM instruments that are in operation or are being developed across the entire range of the EM spectrum will be important. Additionally, the possibility of capturing the early EM emissions can be provided through low-latency alerts; this will require fast response EM instruments. A range of such instruments from high to low energy will be fully discussed in Section 4.

This paper will investigate the types of breakthrough science that will be possible through the low-latency detection and localization of BNS GW events, in particular, how these will enable prompt GW–EM observations of BNS coalescence in the era of advanced detectors. While the science of GW–EM astronomy has been widely investigated previously for longer time-scale EM emissions (e.g. Metzger & Berger 2012; Howell et al. 2015) the feasibility to capture prompt and early EM emissions from binary mergers has not been studied before. To examine the possible EM responses, we use a comprehensive simulation that extends on previous investigations of the early detection and localization of compact binary coalescence (CBC) sources by extensively sampling a range of parameters of the NS waveform and sky localization. We produce statistics showing the expected number of detections and their sky localization error regions at different times before merger. Based on these results, we for the first time extrapolate the temporally complete EM data currently available for short duration gamma-ray bursts (SGRBs) to investigate the capacity of EM instruments for short time-scale EM follow-up observations through the γ-ray, X-ray, optical, and radio. We consider a range of possible emission mechanisms for BNS mergers; some of the possible pathways and end products are illustrated in Fig. 1. Furthermore, our investigation uses the full complement of GW detector network configurations that will be available through the advanced detector era by including KAGRA, LIGO-India, and a proposed Southern hemisphere detector AIGO.

The paper is organized as follows. In Section 2 we describe the framework we use to simulate the GW detection and localization and provide these results in Section 3. In Section 4 we discuss the potential of EM telescopes for rapid follow up observations and in Section 5 provide a review of some of the possible EM emissions that could be captured by prompt observations. Then in Section 6 we use our simulated detection and localization statistics with observational data to determine the astrophysical implications of low-latency GW detection and prompt EM follow up. We then summarize our findings in Section 7.

2 METHODOLOGY

2.1 GW detection

The response of a laser inteferometric GW detector to a GW signal at a given time t is given by

$$h(t) = F_+(t)h_+(t) + F_\times(t)h_\times(t), \quad (1)$$

where F_+ and $F_\times$ are the antenna pattern functions of two independent plus and cross GW polarizations denoted as h_+ and $h_\times$. We adopt the convention of the antenna responses given in Jaranowski, Królak & Schutz (1998). The antenna patterns are expressed as functions of the source sky location – the right ascension α, the declination δ, and the polarization angle ψ. In our simulation, we calculate the waveform $h_+(t)$, $h_\times(t)$ using the second-order PN expansion. It is a function of 11 parameters: the luminosity distance of the source r, the orbital inclination angle ι, the coalescence phase ϕ_c, masses and spins (three parameters for each spin) of these two inspiral bodies. In this paper we only consider non-spinning BNS coalescence.

Matched templates are constructed from the CBC parameter space to perform filtering on the detector data to search for and extract GW signals (Finn 1992). The output of matched filtering is the signal-to-noise ratio (SNR), from which a selection criterion is applied to yield credible GW triggers. Throughout this paper we assume that our detections yield an optimal SNR for each source; that is we assume the template matches the source exactly.

For a network of detectors, two strategies can be considered to select GW candidate triggers. The coincident selection criteria (which we refer to as the triggering criteria in the later part of the paper) require at least two detectors to detect signals above a predefined SNR threshold. A coherent selection criterion assumes that data from different detectors form coherent responses from the source; thus a single statistic is produced and applied against a threshold for trigger generation.

2.2 Latency of GW event triggers

The latency of a GW detection pipeline is defined as the time elapsed from when the source has sufficient SNR for detection to the time

Downloaded from https://academic.oup.com/mnras/article-abstract/459/1/121/2608842 by Universiteit van Amsterdam user on 03 July 2020

Table 1. The workflow of a low-latency CBC detection pipeline showing the latencies achieved in science and engineering runs as well as a projected optimistic latency. The LIGO S6–Virgo VSR2/VSR3 joint observing run was performed during 2009–2010; ER5 and ER6 were engineering runs used to streamline data analysis pipelines by simulating the environment of a real science run.

Process	Latency in S6–VSR2/VSR3 joint run	ER5/ER6 latency	Optimistic latency
GW data acquisition, calibration and distribution	1 min	∼10 s	O(1) s
GW trigger generation	2–7 min	∼40 s	O(1) s
Follow-up preparation	2–3 min	∼60 s	O(1) s
Human vetting	20–30 min	N/A	0 s[a]

[a]This assumes that vetting can be eliminated through automatic processing.

it is registered in the GW event data base.[2] Table 1 outlines the workflow of a typical low-latency CBC pipeline showing the latencies achieved in the LIGO S6–Virgo VSR2/VSR3 joint observing run, the ER5 and ER6 engineering runs, and a projected optimistic pipeline.

The workflow was first practiced in the latest joint LIGO/Virgo science run (Abadie et al. 2012) and the latency is shown in the second column of Table 1. In this process detector data were acquired, conditioned, and distributed. Candidate triggers including CBC triggers were generated by different low-latency GW search pipelines and submitted to the data base. Significant events were then selected and validated manually to form alerts to participating EM observatories. The total time lag was of order 30 min of which 20 min consisted of human validation. The third column of Table 1 shows the results of a recent engineering run with low-latency pipelines specific to search for CBC signals and the final column shows estimated optimistic latencies possible in the future.

GW detector data are first acquired onsite and calibrated and distributed to the computing node where search pipelines are running. From the latest engineering runs, this process takes of order 10 s. In principle, there is no intrinsic obstacle preventing this procedure to achieve minimal latency. Therefore, we assume in the most optimistic scenario that data can be packed, calibrated and distributed within O(1) s.

At the time of writing, three low-latency GW search pipelines have been implemented for the LIGO–Virgo collaboration to search for CBC signals (Buskulic et al. 2010; Abadie et al. 2012; Cannon et al. 2012; Hooper et al. 2012; Luan et al. 2012). These three search pipelines have all achieved an average of around 40 s latency from the time of data acquisition to trigger registration. This latency is mainly due to the processes of data whitening, filtering, and coincident analysis. By employing high-performance computing hardware such as graphic processing units (GPUs) (Chung et al. 2010; Liu et al. 2012) and new high-performance algorithms, this latency could be further reduced. We assume in the future O(1) s latency for filtering and trigger generation from multiple detectors can be achieved in the most optimistic case.

The third row of Table 1 shows the latencies introduced through follow-up preparation, which includes the gathering of event parameters, e.g. sky localization and calculating telescope tilings. The main latency of this part comes from event localization. A low-latency localization pipeline BAYSTAR[3] has been developed and tested (Singer & Price, in preparation) and has achieved latencies in localization of seconds; the run time of this method is shown to be almost perfectly proportional to the number of CPU cores. Thus this latency could be largely reduced and in the optimistic scenario we assume O(1) s latency for this procedure.

[2] GRACEDB: the Gravitational Wave Candidate Event Database.
[3] BAYESian TriAngulation and Rapid localization.

Human vetting introduces the highest latency as the first detections need to be validated carefully. It is natural that once enough detections have been recorded, the knowledge gained will allow this part of the routine to be eliminated by vetoing candidates automatically. We therefore estimate O(1) s for the optimistic case.

In summary, we consider several latency scenarios that include both GW detection and localization for GW triggering: an ideal zero latency and latencies of [1, 10, 40 s] which takes into account the range of extreme to plausible latencies to send out a GW trigger. In Section 5, our discussion is focused on a latency of 40 s which is achievable in the coming science runs and an optimistic latency of 1 s.

2.3 Sky localization accuracy

To determine the localization accuracy of the detected GW events, we utilize the formalism of Wen & Chen (2010) who used the Fisher information matrix to derive a geometrical expression for sky localization accuracy. According to the Cramér–Rao bound (Cramer 1946), the lower bound of the variance of any unbiased estimator is determined by the inverse of the Fisher matrix $\mathbf{\Gamma}$. Using this property, one can calculate the lower bound on the localization error area. This estimation is applicable to any unbiased estimators and to all GW waveforms. This method is also used in Schutz (2011) for a sky localization comparison of different detector networks.

Wen & Chen (2010) presented angular resolution formulae for two different detection scenarios: a best case scenario assumed that the waveform was known but the arrival time was unknown; a worst case scenario assumed that both these quantities were unknown. The calculations include both phase and amplitude information of the signal. The angular resolutions derived from the best case scenarios were shown to be around half the areas of those determined assuming the worst case scenario (Chu et al. 2012). In this paper, we assume the best case scenario to calculate angular resolution for each detection. This is given as

$$\Delta\Omega = 4\sqrt{2}\pi c^2 \sqrt{\frac{(\sum_i \xi_i)^2}{\sum_{\mathrm{J,K,L,M}} \xi_\mathrm{J}\xi_\mathrm{K}\xi_\mathrm{L}\xi_\mathrm{M} |(\boldsymbol{r}_\mathrm{KJ} \times \boldsymbol{r}_\mathrm{ML}) \cdot \boldsymbol{n}|^2}}, \qquad (2)$$

with $\boldsymbol{n}$ the direction of the source which is a function of right ascension α and declination δ and $\boldsymbol{r}_\mathrm{KJ}$ the distance vector from detector K to detector J; the quantity $\xi_i = \int_{-\infty}^{\infty} f^2 |z|^2 \mathrm{d}f$ can be interpreted as noise-weighted energy flux received by the ith detector and z is the SNR (as discussed in Section 2.1).

2.4 Monte Carlo simulation

To produce a sample of detection statistics we simulate a population of 20 000 BNS sources. Our Monte Carlo code extends other studies by considering a full complement of parameters for the BNS waveform and the sky location. The values of right ascension α and

Downloaded from https://academic.oup.com/mnras/article-abstract/459/1/121/2608842 by Universiteit van Amsterdam user on 03 July 2020

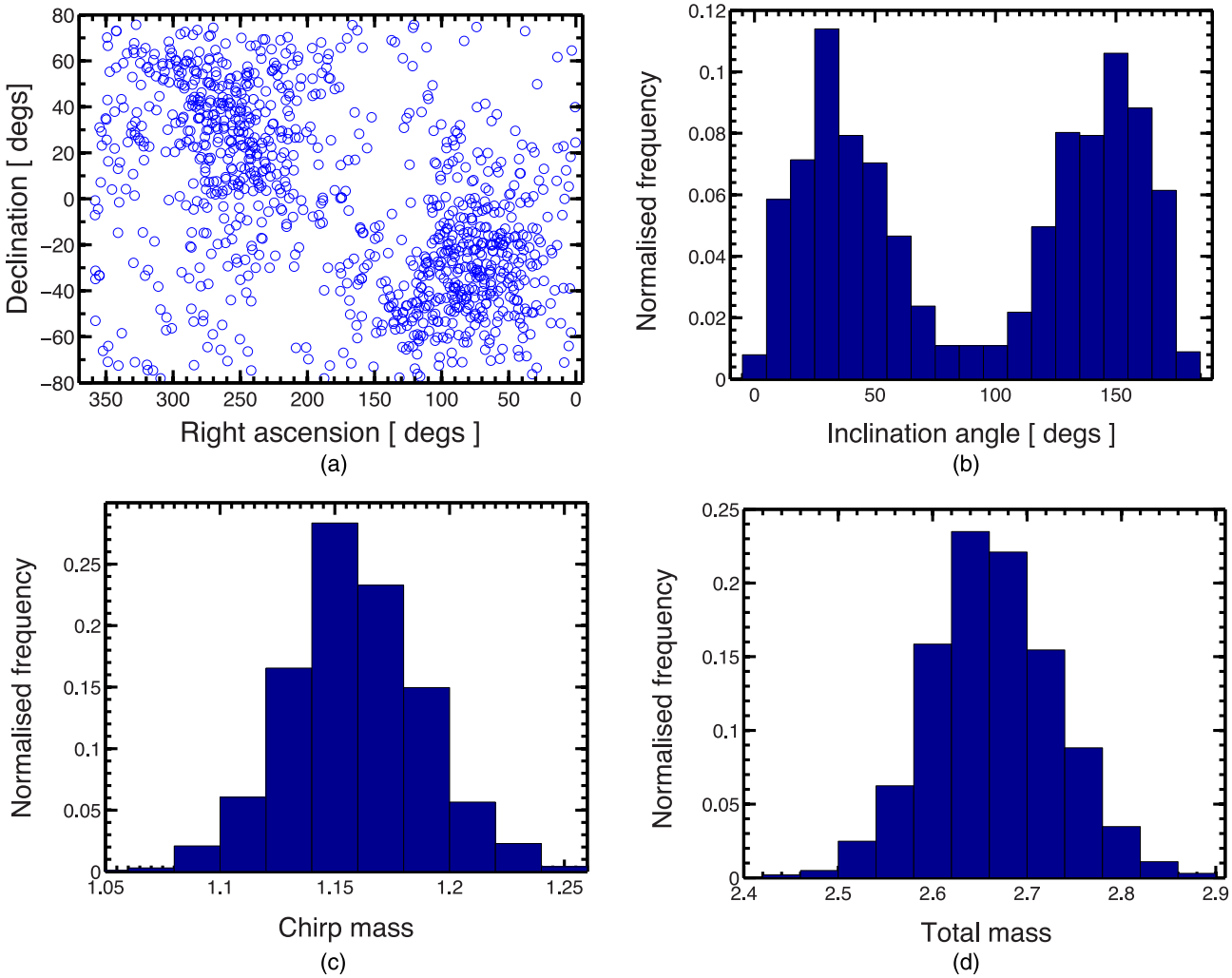

Figure 2. The parameter distributions for the detected sample of sources. We show the distributions of (a) sky location; (b) inclination; (c) chirp mass; and (d) total mass.

polarization angle ψ are draw from a uniform distribution within the range $[0, 2\pi]$. Values for the declination δ angle and inclination angle ι are drawn from a distribution of cosine values uniformly distributed over the range $[-1, 1]$. For each event a source distance r is chosen from within [10, 500] Mpc; this range encompasses the horizon distances of 428 Mpc for aLIGO, 332 Mpc for AdV, and 322 Mpc for KAGRA. For the component masses of each event we assume a Gaussian distribution based on the study of Özel et al. (2012); this study suggests that the mass distribution of BNS systems peaks around 1.33 $M_\odot$ with a standard deviation of 0.05 $M_\odot$.

It is expected that the aLIGO-Livingston (denoted L), aLIGO-Hanford (H), and AdV (V) detectors will reach their full sensitivities around 2019. To model the sensitivities of the advanced LHV detector network, we use the 'zero tuning, high power' spectral density noise curve of LIGO Scientific Collaboration (2009) for aLIGO-Livingston and aLIGO-Hanford; for AdV we use the spectral density curve of Punturo (2012).

Our triggering selection criteria requires a SNR of 7.5 in at least two detectors.[4] This is equivalent to 91 per cent of the reach of a single aLIGO detector triggering off an SNR of 8; this also translates to a 194 Mpc horizon distance. Assuming there will be tens of detections of an LHV network per year, we present our detection estimates as percentages – this allows the statistics for different thresholds to be easily obtained through scaling.

We obtained a total of 1010 LHV coincident detections from our simulated population of 20 000 sources. For an enlarged detector network we assume the same coincident threshold. The key statistics will be presented in Section 3.3. We note that some studies have used a coherent analysis threshold to select sources, e.g. Schutz (2011). The coincident selection thresholds shown here can be simply converted to corresponding coherent analysis thresholds via the detection volume. The statistics of detections from coherent analysis should be similar to the statistics of detections shown in the following section.

3 RESULTS FOR GW TRIGGER EVENTS

3.1 Parameter distributions of detected GW events from LHV network

Fig. 2 shows the distributions for the different parameters of the 1010 simulated BNS detections for an LHV network in the advanced era. Fig. 2(a) shows that the distribution of detected sky locations

[4] We note here that the detection pipeline GSTLAL is configured to use a single detector threshold SNR of 4.

Downloaded from https://academic.oup.com/mnras/article-abstract/459/1/121/2608842 by Universiteit van Amsterdam user on 03 July 2020

is bimodal. The locations of maxima and minima are consistent with the landscape of the antenna power pattern of a LHV detector network (e.g. fig. 2 in Nissanke et al. 2010). As shown in several studies (Nissanke et al. 2010; Schutz 2011; Manzotti & Dietz 2012) adding more detectors to GW search will significantly improve sky coverage.

The distribution of detected inclinations shown in Fig. 2(b) is bimodal and shows a detection preference towards low inclination angles. We note however that the fraction of detected inclinations below 25° is less than one quarter (see also Schutz 2011). The distributions of the chirp mass and total mass of sources are shown in Figs 2(c) and (d).

3.2 The localization of BNS detections

In this section we present the localization evolution statistics for the LHV detections and for an extended detector network that covers the entire parameter space of possible BNS sources. There is a crucial interplay between sending out a prompt alert to an EM facility and surveying the GW error region before the EM source fades. An early trigger can allow a telescope to get on source, but at the expense of a larger GW error region. The situation will vary significantly for different types of telescope and is also dependent of the type of EM emission. In preparation for the later analysis of EM follow-up in Section 6 we have calculated the percentage of sources detectible within different sized error regions at different times before merger. We note that previous studies have calculated the evolution of the localization property with time using a qualitative analysis (e.g. Cannon et al. 2012) rather than the quantitative approach adopted in this paper.

Fig. 3 displays the percentile charts for the evolution of network SNR (Fig. 3a) and localization error area (Fig. 3b) for the 1010 LHV detections as they approach merger ($t = 0$). The network SNR is calculated as root-sum-square of individual SNRs. The plot shows that the median network SNR (thick solid line) is less than 5 at 100 s before coalescence. This SNR increases by 1 every 10 s during −100 to −10 s and by 0.5 every second during −10 to −1 s before reaching a SNR of 16 at merger. We find that 10 per cent of the detections will yield a SNR greater than 27 at merger time which corresponds to a localization area of around 5 deg^2.

Fig. 3(b) shows the percentile range of localization error areas at 90 per cent confidence level as a function of time before merger. On average, the angular resolution is about 30 000 deg^2 at −100 s. As the network SNR increases, this improves to <5000 deg^2 at −40 s, <500 deg^2 before −10 s and less than a hundred square degrees at −1 s. These results support the early localization results of a number of recent studies: see for example Cannon et al. (2012), Manzotti & Dietz (2012) and chap. 3, fig 3.3 of Singer (2015).

3.3 Improved early warning events with a larger detector network

In this section we investigate the benefits of an enlarged GW network in terms of early detection and localization; the scenarios considered are applicable to the advanced detector era beyond 2019. We consider a number of additions to the LHV network: these are KAGRA (labelled as J), the proposed Indian detector: LIGO-India (labelled as I), and AIGO (labelled as A). Though AIGO is not approved financially at the moment, it is considered here for comparison. As in Section 2.4 we use the aLIGO spectral density for LIGO-India and AIGO, and the spectral density from Aso et al. (2013) for KAGRA. The main results are given in Table 2 and Fig. 4.

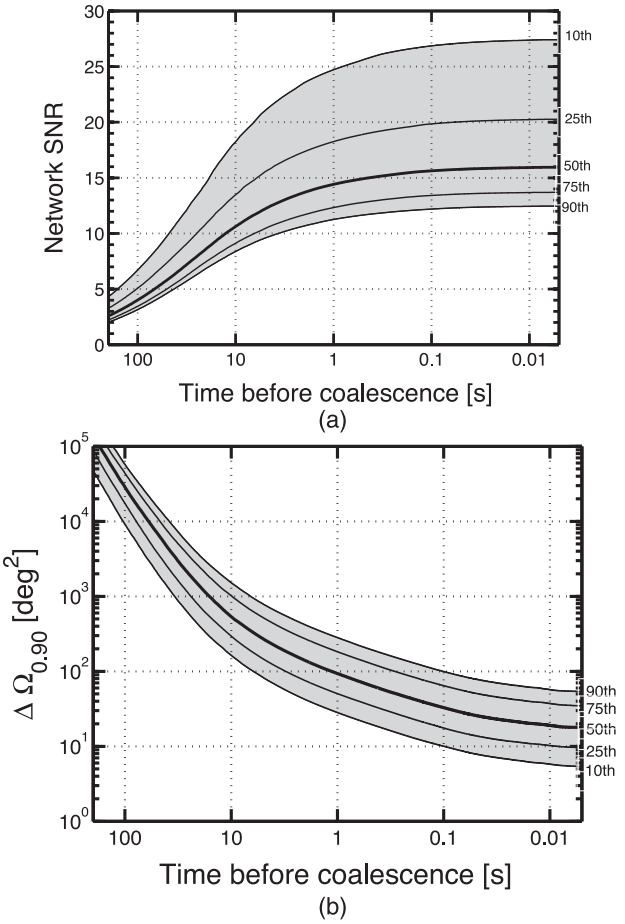

Figure 3. Percentile curves of (a) network SNR and (b) $\Delta\Omega$ (error box at 90 per cent confidential level) as a function of time before merger for the simulated BNS triggers obtained by an LHV network.

The second column of Table 2 shows the detection capability of different detector networks in terms of the number of detections normalized to that obtained from a LHV network (the reference detection capability of LHV is given here as 1.00). For larger network configurations, we find that the detection capability is improved considerably. Using the same coincident triggering threshold for different detector networks, we obtain 1133 detections for LHVJ, 1291 detections for LHVI, 1366 detections for LHVJI, 1280 detections for LHVA, and 1584 detections for LHVJIA. The detection capability of a larger detector network depends on the sensitivities of the additional detectors. We find that adding a single detector with the same detection capability as aLIGO to the LHV network will increase the detection rate by about 30 per cent while adding KAGRA to the LHV network will improve the detection rate by 12 per cent as the sensitivity of KAGRA is 0.75 of that of aLIGO. The detection percentage for each network at different times of the final merger phase is shown in the first row for each network configuration.

Table 2 also shows localization achievable at exact times before merger for different GW network configurations. We illustrate this by showing the sizes of the error regions required to contain 10, 50, and 90 per cent of the detections. All the error region numbers are estimated at the 90 per cent confidential level. We find that adding a KAGRA or LIGO-India instrument to the LHV network can

Downloaded from https://academic.oup.com/mnras/article-abstract/459/1/121/2608842 by Universiteit van Amsterdam user on 03 July 2020

Table 2. The detection statistics obtained for different advanced detector networks shown in the first column. The second column shows the relative detection capability of each network in comparison to LHV. Columns 4–7 provide two sets of statistics at different times before merger for each detector network: in the first row we provide the percentage of detections achieved pre-merger; the second row gives the sizes of the error regions required to contain 10, 50, and 90 per cent of the detections at exact times before merger.

Network	Detection capability		Time before merger 40 s	10 s	1 s	0 s
LHV	1.00	Percentage detected	9 per cent	35 per cent	76 per cent	100 per cent
		(10/50/90 per cent) error regions (deg^2)	300/1000/2200	70/270/780	20/80/240	5/20/50
LHVJ	1.12[a]	Percentage detected	8 per cent	32 per cent	76 per cent	100 per cent
		(10/50/90 per cent) error regions (deg^2)	240/820/1600	50/200/470	10/40/120	3/10/30
LHVI	1.28	Percentage detected	9 per cent	33 per cent	75 per cent	100 per cent
		(10/50/90 per cent) error regions (deg^2)	120/380/910	40/130/350	10/40/100	3/9/20
LHVA	1.27	Percentage detected	9 per cent	35 per cent	76 per cent	100 per cent
		(10/50/90 per cent) error regions (deg^2)	80/310/850	30/90/250	9/30/80	2/6/20
LHVJI	1.35	Percentage detected	8 per cent	32 per cent	75 per cent	100 per cent
		(10/50/90 per cent) error regions (deg^2)	100/340/830	30/110/300	9/30/80	2/7/20
LHVJIA	1.57	Percentage detected	9 per cent	33 per cent	75 per cent	100 per cent
		(10/50/90 per cent) error regions (deg^2)	60/180/400	20/60/140	6/20/40	1/4/10

[a]This number is lower than that of LHVI/LHVA network as the sensitivity we adopted for detector J is 0.75 of that of detector I/A.

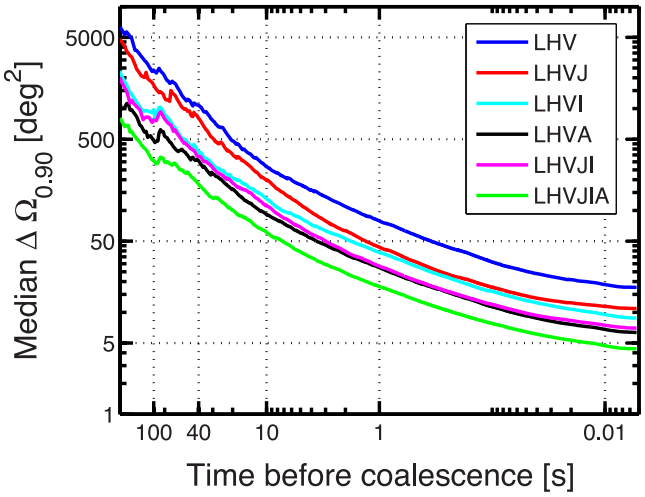

Figure 4. Median localization error areas of detections at exact times prior to merger for different detector networks. The fluctuations seen at early times are due to the smaller number of detections in that regime.

improve the localization by a factor of 2. Increasing the network to five detectors can lead to a factor of 3 improvements. Adding AIGO on its own results in an improvement that is equivalent to adding both KAGRA and LIGO-India due to the longer baseline and optimal location. Adding AIGO to the five-detector network can further improve the localization by a factor of around 2 – this is a factor 5 improvement over the initial LHV network.

An important fact is that only a fraction of detections can be detected at times prior to merger. We take this into consideration and show the localization error area for the detections at different times prior to merger. Fluctuations of localization error area at early times in Fig. 4 are due to small number of detections in that epoch. We note our estimated localization error areas determined near merger time are comparable, though slightly more optimistic than Fairhurst (2011) and Aasi et al. (2013). Whilst the aforementioned studies used the Fisher matrix for the triangulation localization method, our estimates are based on the Fisher matrix regardless of the localization method, thus represent a lower limit of all non-biased estimations.

In practical terms, the latencies introduced in the GW–EM effort will affect the timing of the EM follow-up observation and therefore constrain the phenomena we are able to observe. Using Table 2, one can easily consider different GW–EM reaction latency scenarios and find the detection ratio and localization error area for follow-up observations at merger or at post-merger time-scales. For example, assuming a 40 s total reaction latency – incorporating the whole GW trigger generation and EM follow-up readiness latencies – can be achieved, those GW events that pass the GW triggering criteria 40 s before the merger can potentially be observed right at their merger time by EM instruments with wide FoVs and rapid responses. For the LHV network, which is expected to be operational at early stage of advanced era, around 9 per cent of all detections can be observed at the merger time within 40 s. The median localization error area of the detections at the merger time is over 1000 deg^2. The median localization error area can be brought down to about 400 deg^2 by an LHVI detector network and 10 per cent detections of LHVI network at the merger time could be localized within 120 deg^2. With a five-detector network, 10 per cent of the detections could be discovered and localized within 100 deg^2 at the time of merger.

If a greater effort could reduce the total reaction latency to 10 s (this highly optimistic scenario would require an EM facility to be on source), the detection ratio at the merger time will be raised to around 33 per cent for the six networks which is three times the observed detections at 40 s latency. More importantly, the localization accuracy is also three times better than that achieved with 40 s latency. For the LHV network, the median localization area is improved fourfold to 270 deg^2 and 10 per cent of detections could be localized within 70 deg^2. Adding KAGRA or LIGO-India into the LHV network will improve the localization to less than 50 deg^2 for 10 per cent of their detections. The localization accuracy will be further brought down to about 30 deg^2 for a network of LHVA or LHVJI of 10 per cent of their detections. The best localization accuracy comes at an operation of six detectors with around 90 per cent of the detections localized to within 140 deg^2. We consider further the possibilities of existing EM facilities in the next section.

Downloaded from https://academic.oup.com/mnras/article-abstract/459/1/121/2608842 by Universiteit van Amsterdam user on 03 July 2020

Table 3. The properties of some of the high-energy instruments planned to be operational during aLIGO.

Instrument	Energy range	FoV (deg^2)	Sensitivity ($erg\,s^{-1}\,cm^{-2}$)	Exposure time	Response time	Ref
Swift-BAT	15–300 keV	4600	1.2×10^{-8}	–	Coincident observation	[1]
Swift-XRT[a]	0.3–10 keV	0.15	6×10^{-12}	10	1–2 h	[1]
Fermi-GBM	8 keV–40 MeV	30 000	4×10^{-8}	–	Coincident observation	[2]
Fermi-LAT[b]	0.02–300 GeV	8000	1.4×10^{-7}	100 s	30 s post-GBM trigger	[2]
CTA[c]	0.03–100 TeV	6–8	6×10^{-9} at 25 GeV	1000 s	20–60 s	[3]
CTA (Survey mode)[d]	0.03–100 TeV	∼1000	6×10^{-8} at 25 GeV	1000 s	20–60 s	[3]
H.E.S.S.[c]	0.05–20 TeV	15	$\sim 6 \times 10^{-8}$ at 25 GeV	1000 s	30 s	[3]
SVOM-ECLAIRS	4–250 keV	89	7.2×10^{-10}	1000 s	∼1–2 h	[4]
SVOM-MXT	0.2–10 keV	64 arcmin	5.6×10^{-11}	10 s	∼1–2 h	[4]

Notes. Ref: [1] Gehrels et al. (2004); [2] Meegan et al. (2009); [3] Bartos et al. (2014); [4] Götz et al. (2014).
[a]Sensitivity approximated using Zhang (2013) equation (3) $F_{\rm x,\,th} = 6 \times 10^{-12}/T_{\rm obs}$ erg s^{-1} cm^{-2} and assuming $T_{\rm obs} = 10$ s.
[b]Sensitivity over 100 s estimated using fig. 2. of Atwood et al. (2009) and converted to erg s^{-1} cm^{-2} using a standard band function with $\alpha = -1$, $\beta = -2.25$, and $E_{\rm P} = 511$ keV.
[c]Approximated using Funk et al. (2013).
[d]Sensitivity in survey mode based on [3] in which exposure time includes an estimate of the required slewing times to tile a 1000 deg^2 area using convergent pointing mode.

4 EM TELESCOPES FOR PROMPT GW FOLLOW-UP OBSERVATIONS

In this section we will discuss some of the EM instruments in different EM wavelength bands that will be able to facilitate prompt GW follow-up – we consider a selection from those that currently have MoUs for aLIGO/AdV follow-ups in place. We focus first on the high energy which is traditionally low latency (usually employing triggering instruments) but will not be fast enough unless there is an agreement for prompt Target of Opportunity (ToO) in place; we note that high-energy observations of GRBs over the last two decades have produced significant science returns in this domain. We then discuss optical telescopes which are proven for low latency through the successful use of fast response instruments for GRB follow-up. Finally, we consider radio which though electronic steering and/or rapid slew-times can make rapid response follow-ups achievable.

4.1 X-ray and γ-ray follow-ups

Table 3 shows the various properties of some of the high-energy instruments with LIGO/AdV MoUs in place.

Space-based γ-ray follow-ups will be led by *Fermi* and *Swift*. These instruments provide the capability for the discovery of simultaneous EM counterparts; in this respect the large FoV of the *Fermi*-Gamma-Ray Burst Monitor (GBM), which sees almost the entire unocculted sky can be advantageous. A typical follow-up procedure will be to search through the data for a coincident signal from a location of the sky consistent with the LIGO error region. Assuming coincident [GW/*Fermi* on-board] triggers, the response time will be around a few minutes. If there are no on-board triggers, a sensitive search through the *Fermi* data set will require of order 4–12 h. The *Fermi*-Large Area Telescope (LAT) can provide more information of the high-energy afterglow. Typically the LAT autonomously re-points after a GBM trigger with a processing delay of around 30 s. If no on-board trigger is available, a ground-based search of the data can be initiated; the latency will depend on the time between the GW candidate and the data downlink[5] and processing, of order one to a few hours.

The *Swift* γ-ray instrument is a wide-field (1.4 sr) coded mask hard X-ray imager [Burst Alert Telescope (BAT)]. Although the *Swift*-BAT is more sensitive than the *Fermi*-GBM, it observes softer γ-rays; this last point is important for *Fermi*-GBM, follow-ups as SGRBs associated with BNS mergers have harder spectra than long duration gamma-ray bursts (LGRBs).

In terms of identifying transients, follow-ups in the X-ray have the advantage of a less crowded sky than that of the optical. For X-ray follow-ups the *Swift*-X-Ray Telescope (XRT) rapid slew time is particular advantageous; this has resulted in this instrument accumulating around 200 GRB redshifts though coordinated observations with ground-based telescopes. The *Swift*-XRT is able to respond rapidly to a BAT detection of new transient, localizing to within 1–3 arcmin and then distributing the position via the Gamma-ray Coordinates Network (GCN) within a 20-s window.

Swift demonstrated the feasibility of rapid high energy ToO follow-ups by conducting the first multiwavelength follow-up observation during the 2009–2010 LIGO/Virgo science run (Evans et al. 2012). *Swift* followed-up and observed the sky locations for two candidate GW events within 12 h, using a specially designed strategy to target the most probable positions that the GW event originated from. To improve ToO requests with large positional uncertainties, *Swift* implemented tiled XRT observations in late 2011. However for this instrument, at the present time, a response time to ToO of order 1–2 h (Kanner et al. 2012) by the on-board XRT effectively rules this instrument out in terms of low-latency follow-ups. If however, in the future, aLIGO could send triggered alerts directly to *Swift* without human intervention, a slew of order 10 s of seconds would result in early follow-up observations of the X-ray light curve.

In addition to the *Swift*-XRT, Astrosat,[6] an Indian multiwavelength satellite was successfully launched in 2015 September. Astrosat has instruments covering the UV (UVIT), optical, soft and hard X-ray [the Cadmium Zinc Telluride Imager (CZTI)]. For follow-up operations, once a counterpart is identified, re-pointing will bring the target within the FoV of the other instruments for simultaneous coverage from optical though to hard X-ray. For low-latency follow-ups, CZTI, the hard X-ray coded aperture mask instrument with a 36 deg^2 FoV will be the most useful instrument. As

[5] The communication going from the satellite to the ground.

[6] http://astrosat.iucaa.in/

Downloaded from https://academic.oup.com/mnras/article-abstract/459/1/121/2608842 by Universiteit van Amsterdam user on 03 July 2020

contact with the spacecraft is designed to take place once in an orbital period of 100 min, this is typically is the fastest time-scale over which a slew can be commanded; ToO decision making may also be added to this response time. However, one low-latency scenario exists, in that if there was significant hard X-ray/γ-ray flux in the (100–1000) keV band, the CZTI would detect the flash without repointing. Over this energy range the CZTI acts like an open detector with a 2π FoV; we note however that there will be no localization capability at these energies.

Ground-based gamma-ray detectors can also contribute to the GW follow-up effort through the Cherenkov Telescope Array (CTA; Dubus et al. 2013). The CTA is a next generation ground-based instrument that will begin construction around 2016, with full operation expected by 2020. CTA will improve over previous experiments(H.E.S.S, VERITAS[7] and MAGIC[8]) through increased sensitivity, angular resolution ($\sim$2 arcmin at TeV), wider energy coverage ($\sim$30 GeV–300 TeV) and a larger field of view (6°–8°). This project will consist of two arrays: a southern hemispheric array focusing on Galactic sources and a northern hemispheric array on extragalactic. Bartos et al. (2014) has recently highlighted some of the properties that make this instrument ideal for GW follow-up. These include the capability to observe in a pointed mode with a relatively small FoV and in survey mode covering a larger area large sky area ($\sim$1000 deg^2); fast repositioning is of the order of a few seconds (Doro et al. 2013). For low-latency follow-ups the ability to respond to ToO requests and start monitoring the GW error ellipse within 30 s is significant (Dubus et al. 2013).

CTA is designed to have three types of telescopes with different mirror sizes to cover the full energy range – large-scale telescopes (24-m) covering <300 GeV, medium scale (10–12 m) covering 100 GeV–TeV and small-scale (4–6 m) covering higher energies >10 TeV. Typically, extragalactic background light (EBL), which is all the accumulated radiation in the Universe due to star formation processes, will attenuate very high energy photons coming from cosmological distances through pair production with EBL photons. This produces the effect in that only the large-scale telescopes will be triggered. However, for the case of a GW source within 200 Mpc, TeV photons are not expected to be annihilated (Bartos et al. 2014); thus all three types of CTA telescopes CTA could be triggered (O'Brien & Hinton, personal communication) providing a greater energy coverage.

H.E.S.S.,[9] an array of five Cherenkov telescopes (with 4 $\times$ 12 m and one 28-m diameter mirrors) located in Namibia, has been operational since 2004. This telescope has a mean time to get on source from a random observation position of about 30 s (Lennarz et al. 2013). The capability of H.E.S.S. for GW follow-ups has been proven through prompt observations of GRB triggers. A follow-up observation of GRB 070621 was achieved within 7 min (Aharonian et al. 2009) and GRB 100621A was observed within 10 min.

4.2 Optical follow-ups

Optical follow-ups have been hugely successfully in the last decade to discover the afterglows and host galaxies of GRBs. For *Swift* follow-ups, this strategy has relied on the prompt localizations of the XRT and the rapid distribution of coordinates via the GCN network. Recently, robotic optical telescopes have been able to identify the optical afterglows of *Fermi*-GBM triggers that have large positional uncertainties (e.g. GRB 130702A; Singer et al. 2013, 2015). A successful low-latency EM follow up to a GRB could potentially capture an optical flash or the earliest stages of a particularly bright rising afterglow.

Table 4 lists the capabilities of a number of optical instruments that will be available during the era of advanced GW detectors. Capturing an EM counterpart with such a fast response will be dependent on a number of factors related to the telescope. The FoV of the instrument will determine how quickly the GW localisation area can be surveyed (i.e. the number of tiles required); any subsequent detection will then be dependent on the limiting magnitude or sensitivity of the instrument and on the required exposure time to obtain the required sensitivity (for an in depth discussion see Coward et al. 2014).

For prompt follow-up, the slew time of the instruments will be highly important; for telescopes with lower sensitivities a rapid slew time can compensate through the ability to achieve pointing during the brightest part of the event. However, we note here that for optical instruments, a fast slew time is usually associated with a small FoV.

Fast response optical telescopes such as TAROT have the ability to slew to a target position within 10 s. However, the FoV $\sim$3.5 deg^2 and exposure time of around 60 s mean that time must be allowed to image the full error region. Assuming a 60 deg^2 error box, corresponding to that of a LHVJIA network at 50 per cent confidence, using the framework presented in Coward et al. (2014), we find the imaging time will be of order 17 min. Larger FoV telescopes would be able to minimize the required imaging time. For example, Pan-STARRS, a system of four automated 1.8-m optical telescopes based in Hawaii has a FoV of $\sim$7 deg^2 and an exposure time of 30 s yielding a 4 min response for the same error box. The Zwicky Transient Facility (ZTF)[10] will be an extension of the Palomar Transient Factory (PTF; 7 deg^2 FoV) with an increased 47 deg^2 FoV and an order of magnitude improvement in survey speed. GOTO,[11] a dedicated optical follow-up instrument with a proposed initial configuration of 18 deg^2 instantaneous FoV will require an exposure time of around 5 min to reach 21 mag (Steeghs & Galloway, personal communication); however, for this instrument a shallower inventory of the large error ellipses may be possible. Additionally, BlackGEM,[12] expected on-line from 2016, aims to cover 40 deg^2 in a seeing-limited configuration with an exposure time of 5 min (Ghosh & Nelemans 2015).

Considering the FoVs given in Table 4, it is immediately apparent that for fast response observations, unless a wide FoV instrument is on-source, one may require a larger network than LHV to decrease the localization error (Manzotti & Dietz 2012) and thus, reduce the number of tiles required to image the full GW error box.

In addition to the facilities outlined in Table 4, a number of other facilities are in development for GW follow-up and could be operational during the later era of aLIGO/AdV. One such facility is RAMSES which will consists of a set of 16 $\times$ 40 cm telescopes and will be equipped with rapid cameras capable of readout times from 100 ms to several minutes; it will be able to reach magnitudes of 15 in 1 s and magnitudes 20 within around 10 min. Each telescope has a 2.5 deg^2 FoV, resulting in a combined 100 deg^2 FoV; this in combination with a slew time of around 5 s would enable instantaneous coverage of a large proportion of a typical aLIGO/AdV error region.

[7] http://veritas.sao.arizona.edu/
[8] http://magic.mppmu.mpg.de/
[9] http://www.mpi-hd.mpg.de/hfm/HESS/
[10] http://www.ptf.caltech.edu/ztf
[11] http://goto-observatory.org/
[12] https://astro.ru.nl/blackgem/

Downloaded from https://academic.oup.com/mnras/article-abstract/459/1/121/2608842 by Universiteit van Amsterdam user on 03 July 2020

Table 4. The properties of a selection of the optical telescopes planned to be operational during aLIGO.

Telescope	FoV (deg^2)	Limiting magnitude *R* band	Exposure	Ref
TAROT	3.5	18	60 s	[1]
SkyMapper	5.7	21	110 s	[2]
Zadko	0.15	21	180 s	[3]
Pan-STARRS	7.0	24	30 s	[4]
GOTO	18.0–36.0	21	5 min	[5]
BlackGEM	40.0	22	5 min	[6]
Zwicky Transient Facility (ZTF)	47	20.5–21	30 s	[7]
Ground-based Wide-Angle Camera (GWAC)	8000	16	10 s	[8]

Notes. Ref: [1] Klotz et al. (2013); [2] Keller et al. (2007); [3] Coward et al. (2010); [4] Hodapp et al. (2004); [5] Steeghs & Galloway (personal communication); [6] Ghosh & Nelemans (2015); [7] Smith et al. (2014), Bellm (2014); [8] Paul et al. (2011).

Table 5. The capacity of radio telescopes in consideration. Ref: [1] Tingay et al. (2013); [2] Murphy et al. (2013); [3] van Haarlem et al. (2013)[a]; [4] Oosterloo, Verheijen & van Cappellen (2010).

Name	Frequency range	FoV	Limiting flux density	Response time	Ref
MWA	80–300 MHz	610 deg^2 at 150 MHz	20 mJy	<10 s	[1]
ASKAP	700 MHz–1.8 GHz	30 deg^2 at 1.4 GHz	640 μJy $beam^1$ (10 s int)	<min	[2]
LOFAR LBA (inner)	10–90 MHz	450 deg^2 at 60 MHz	5 mJy at 60 MHz	<min	[3]
LOFAR HBA (core)	110–250 MHz	48 deg^2 at 180 MHz	0.6 mJy at 180 MHz	<min	[3]
APERTIF	1–1.7 GHz	8 deg^2 at 1 GHz (>100 deg^2)[b]	0.1 μJy		[4]

[a]LOFAR sensitivities quoted for an observation comprising of a total bandwidth of 7.8 MHz and a 1 h integration time assuming six subarray pointings are created, calculated using http://www.astron.nl/~heald/test/sens2.php
[b]APERTIF will be able to cover 100 deg^2 at lower sensitivity in a 'fly's eye' mode.

RAMSES has received funding and will be based in National Aures Observatory in Algeria[13] with a prototype built in France.

4.3 Radio follow-up

Table 5 provides specifics for some of the radio instruments that have signed MoUs with LIGO/AdV. A period of significant investment in facilities and infrastructure and advances in high-speed computing over the last few years will enable this band to make a telling contribution to time-domain astronomy. The instruments included in this table have the potential to be leading transient detectors by virtue of their large FoV, high sensitivity and significantly for low-latency follow-ups, the capability to respond from 10 s of seconds up to within a minute. The triggering methodology has already been implemented by the Arcminute Microkelvin Imager (AMI; Staley et al. 2013) who have demonstrated typical response times for follow-up of *Swift*-BAT triggers of order 5 min.

The ASKAP[14] Survey for Variables and Slow Transients (VAST; Murphy et al. 2013) is a Survey Science program that will operate in Western Australia. Phased array feed technology on each of 36 antennas 12-m diameter will allow an instantaneous FoV of 30 deg^2 at 1.4 GHz, with a resolution of 10–30 arcsec at 300 MHz bandwidth, and a frequency range of (0.7–1.8) GHz. The VAST transient detection pipeline will operate on an imaging cadence of 5–10 s at its fastest down to a cadence of minutes depending on available supercomputing resources. Longer cadences of hours to months can also be conducted through repeated observations of selected fields. When commissioning is complete, ToO response time-scales could be as short as minutes when operating in fully automated mode. This accompanied by the large FoV could provide good follow-up opportunities for very low-latency triggers.

In the Netherlands, APERTIF (e.g. Verheijen et al. 2008; Oosterloo et al. 2010) will significantly increase the FoV of the Westerbork Synthesis Radio Telescope and will operate at 1.4 GHz. In standard observing modes, the field of view will be 8 deg^2, but has the potential to be extended to 100 deg^2 in a 'fly's eye' mode (Oosterloo et al. 2010).

The Murchison Widefield Array (MWA; Tingay et al. 2013) is a Western Australia-based low-frequency radio telescope operating between 80 and 300 MHz. It consists of 2048 dual-polarization dipole antennas arranged as 128 tiles. The array has no moving parts, and pointing is achieved by electronically steering.[15] This provides the ability to retroactively point, at a reduced sensitivity, to a location on the sky in response to a GW event trigger. In addition, implementation of a VOEvent triggering pipeline will reduce the response of this instrument to tens of seconds (Kaplan, personal communication).

The MWA's large FoV – 600 deg^2 at 150 MHz defined by the full width at half-maximum (FWHM) of the primary beam – can be extended to 1600 deg^2 by taking the entire central lobe of the primary beam. At lower frequencies, the FoV scales proportionally to the square of the wavelength, so at 100 Hz one can obtain a FoV ~3600, almost 10 per cent of the celestial sphere at a single pointing (Kaplan, in preparation). Given a sufficient event rate, the MWA could be pointed at a single patch of sky guaranteeing that 10 per cent of GW triggers would be captured with zero latency. This improved FoV can be augmented by the MWA Voltage Capture System (VCS; Tremblay et al. 2015) which would allow data to be simultaneously collected in a 2 s cadence imaging mode and in

[13] http://www.craag.dz/
[14] Australian SKA Pathfinder (ASKAP; Johnston et al. 2007).
[15] Telescope functions including pointing are performed by electronic manipulation of dipole signals.

Downloaded from https://academic.oup.com/mnras/article-abstract/459/1/121/2608842 by Universiteit van Amsterdam user on 03 July 2020

continuous voltage data collection mode. The VCS can be used as a deep disc-based ring buffer with a 1 h duration. On receipt of a GW trigger, voltage data around the on-source window could be siphoned off for post-trigger analysis.

The Low Frequency Array (LOFAR; van Haarlem et al. 2013) is an interferometric array of dipole antenna stations distributed throughout the Netherlands and several countries in Europe. LOFAR uses two distinct antennas types: Low Band Antennae (LBA) operating between 10 and 90 MHz and High Band Antennae (HBA) operating between 110 and 250 MHz. The antennas are organized in aperture array stations, with initial beam forming conducted on the station level. These stations have no moving parts and electronic beam-forming techniques allow for rapid re-pointing of the telescope. Because of strategies required to manage the high data rates from LOFAR, the FoV is constrained during the initial processing stages; it is highly dependent upon the station configurations chosen and the observing frequency. Larger FoVs can be attained by using shorter baseline configurations but with a loss of sensitivity and resolution. The maximum FoV (whole observable sky when operating with the LBA) will be monitored in a 24 × 7 commensal observing mode by (AARTFAAC)[16] (the Amsterdam-ASTRON Radio Transients Facility and Analysis Centre; Prasad et al. 2014). At the time of writing, LOFAR still requires manual intervention for external triggers. However, the expectation is that VOEvent triggering will be enabled in time for the first LIGO science runs, reduce the latency to less than a minute. In addition, LOFAR are also developing rapid response strategies based around transient buffer boards (van Haarlem et al. 2013) which, similar to the VCS used by MWA, can store small amount of the full observed data for later analysis.

In the longer term, the Square Kilometre Array[17] (SKA) will be provide large fields of view and increased sensitivity, with construction scheduled to start in 2018. SKA phase 1 will compose of two instruments SKA-low, operating at 50–350 MHz, and SKA-mid, operating at 350 MHz–14 GHz.

5 A REVIEW OF EM EMISSIONS FROM BNS MERGERS

A number of associated EM counterparts have been proposed for BNS mergers, many of which have already been presented in Fig. 2. We will begin this section by expanding on the multimessenger pathways and end products provided in Fig. 2 which could produce observable EM counterparts for binary coalescences. We will discuss the various scientific breakthroughs that could be achieved in the advanced detector era through low-latency follow-ups and discuss the type of EM observational bands and facilities that could benefit the most from low-latency GW triggers.

Although the scope is wide, the relative brightness of the associated EM signals is dependent on poorly understood merger physics, in particular that of the post-merger central remnant object. Therefore, the prospects of detecting many of these EM counterparts are quite speculative. To address some of this uncertainty, in the latter parts of this section we use the best available EM data to indicate the possible flux of the possible EM counterparts. We do this in the context of EM telescopes already discussed in Section 4 which will be available for follow-up observations during the aLIGO era.

[16] AARTFAAC will have a FoV of 10 000 deg^2 covering 25 per cent of the sky. See http://www.aartfaac.org/

[17] https://www.skatelescope.org/

Short GRBs have long been proposed to originate from mergers of compact object binaries (Paczýnski 1986, 1991; Eichler et al. 1989; Narayan et al. 1992). Recent broad-band observations have shown mixed host galaxy types, non-detection of supernova associations and offsets of GRB locations from their host galaxies (see Berger 2014, for a review). These findings lend support to compact binary mergers as the progenitors for SGRBs.

Generally the merger of BNSs can produce a number of different products; these can be divided into four categories.

(1) A black hole.
(2) A hypermassive NS supported by differential rotation; this is expected to collapse to a BH within 10–100 ms.
(3) A stable NS that does not collapse.
(4) A supramassive NS supported by rigid rotation; this is expected to collapse to a BH within 10–10000 s with a typical timescale of hundreds of seconds.

If the merger product is of the first two categories: (1) a black hole or (2) a temporal hypermassive neutron star, the EM signals could include the SGRB and its afterglow emission (Eichler et al. 1989; Barthelmy et al. 2005a; Gehrels et al. 2005; Berger 2011; Rosswog, Piran & Nakar 2013) and a long-lasting radio afterglow of the ejecta as it interacts with the ambient medium (Nakar & Piran 2011; Metzger & Berger 2012; Piran, Nakar & Rosswog 2013).

During a NS–NS merger or NS–BH merger, a small fraction of materials are tidally ripped and dynamically ejected. These ejecta are mostly composed of radioactive elements, which would heat the ejecta via decay of r-process nuclei, powering an UV/optical/IR transient (Li & Paczyński 1998; Kulkarni 2005; Metzger et al. 2010; Barnes & Kasen 2013) that has been termed a *kilonova*. Recent optical and near-IR observations of a kilonova associated with GRB 130603B have provided support for this scenario and thus a compact object merger origin of SGRBs (Berger et al. 2013; Tanvir et al. 2013).

It is important to note that the SGRB and its afterglow are relativistic and collimated (Burrows et al. 2006; De Pasquale et al. 2010), so only detectable in preferred directions. Alternatively, the kilonova ejecta and its radio afterglow are essentially isotropic and also non-relativistic (due to the heavy mass loading) and therefore can be detected from any direction if the flux is high enough.

The latter two categories, (3) and (4) can both lead to a magnetar as the merger product; this could occur through a small enough total NS mass in combination with a stiff equation of state of nuclear matter. This could be a stable magnetar (for case 3) or a supramassive millisecond magneter (case 4), which would very likely be strongly magnetized and rapidly spinning (e.g. Dai & Lu 1998; Dai et al. 2006; Fan & Xu 2006; Gao & Fan 2006; Yu & Huang 2007; Giacomazzo & Perna 2013; Hotokezaka et al. 2013; Zhang 2013; Lasky et al. 2014; Ravi & Lasky 2014; Shibata et al. 2014).

Plateaus in the X-ray afterglow light curves of about 60 per cent short GRBs have been attributed to such millisecond magnetar central engines (Rowlinson et al. 2010a, 2013; Lü et al. 2015). The plateau emission of these SGRBs is interpreted as internal dissipation of the magnetar wind due to the dipole spin-down of the magnetar (Zhang & Mészáros 2001; Troja et al. 2007; Metzger et al. 2011). The magnetic spin-down of the NS remnant provides an additional source of sustained energy injection, which greatly enriches the EM signals. A jet may be still launched via accretion from a disc to power the SGRB emission (Metzger, Quataert & Thompson 2008; Dessart et al. 2009; Lee, Ramirez-Ruiz & López-Cámara 2009; Fernández & Metzger 2013). In the SGRB afterglow phase, some observed features, including the extended prompt emission

Downloaded from https://academic.oup.com/mnras/article-abstract/459/1/121/2608842 by Universiteit van Amsterdam user on 03 July 2020

(Norris & Bonnell 2006; Metzger et al. 2008), X-ray flares (Barthelmy et al. 2005b; Campana et al. 2006), and more importantly, plateaus observed in the X-ray are consistent with being powered by a millisecond magnetar central engine.

Outside the solid angle extended by the SGRB jets, several potentially observable astrophysical processes have been predicted. First, self-dissipation of the magnetar wind could power a bright early isotropic X-ray afterglow (Zhang 2013). Next, heating by the magnetar wind (expected to be more significant than the radioactive decay) could significantly enhance the kilonova emission component (Yu, Zhang & Gao 2013; Metzger & Piro 2014). Finally, the magnetar wind could accelerate the ejecta to a mildly or even moderately relativistic speed, giving rise to a strong broad-band afterglow emission upon interaction with the ambient medium (Gao et al. 2013).

Finally, a remarkable new class of extremely bright and short-duration (millisecond time-scale) transients called FRBs could be a product of BNS merger (Lorimer et al. 2013; Thornton et al. 2013). An FRB could be emitted through a BNS merger in two possible ways:

(1) during the BNS merger a coherent radio emission could be produced through magnetic braking as the magnetic fields of the NSs are synchronized in binary rotation at the time of coalescence (Totani 2013);

(2) if a supramassive NS is the merger product, it would collapse into a black hole after losing the centrifugal support and emit an FRB (Zhang 2014) due to the ejection of the magnetosphere as it implodes into the black hole (Falcke & Rezzolla 2014).

The latter scenario is evidenced by an abrupt drop in the X-ray plateau emissions of some long and short GRBs. Within this latter scenario, an FRB along the jet direction is expected after a BNS merger event that forms the supramassive NS.

In the remainder of this section, we will discuss each of the potential electromagnetic counterparts in more depth and compare the expected emission to the capabilities of the instruments described in Section 4. First, in Section 5.1, we outline the methods used to quantify the typical emission we might expect. Section 5.2 considers the on-axis emission expected from our understanding of SGRBs and Section 5.3 discusses the isotropic kilonova counterpart. In Section 5.4 we describe the impact of changing the central engine formed by the BNS merger from a black hole to a magnetar on the standard emission as discussed in Sections 5.2 and 5.3. Finally, in Section 5.5, we consider the possibility of early-time FRBs associated with a BNS merger and how low-latency triggers and existing instrumentation can constrain these predictions.

6 ASSESSING PROMPT EM FOLLOW-UPS FROM LOW LATENCY GW TRIGGERS

6.1 Extrapolation of fluxes for observed EM counterparts

In this section we explore the benefits of low-latency GW follow-up observations by extrapolating observed emissions from known sources associated with BNS mergers to the observational range of ground-based GW detectors. SGRBs are the most likely observed population to be associated with BNS. Therefore, we can estimate the typical fluxes that could be expected at different energies by extrapolating from known SGRBs associated with BNS at a distance of 200 Mpc. The results are shown in Table 6 however, due to the nature of the SGRB observations, these numbers focus on the on-axis emissions. These values are representative of the expected on-axis signals but we do not give the full range of expected fluxes; this requires detailed modelling, beyond the scope of this paper. Where possible, we utilize GRB 130603B as it is the only unambiguously SGRB associated with a BNS merger with a spectroscopic redshift from the optical afterglow (Barthelmy et al. 2013; de Ugarte Postigo et al. 2014; Fong et al. 2014). GRB 130603B does not exhibit the all of the emission combinations we consider and, in those cases, we use other SGRBs with reasonable host galaxy redshift constraints.

The X-ray, γ-ray, and radio flux estimates are obtained by extrapolating to the required observation time from broken power law fits to the light curves of the GRBs, which are converted into rest-frame luminosities using a k-correction and the observed spectral slope (Bloom, Frail & Sari 2001). The observed flux at a distance of 200 Mpc is calculated by converting the rest-frame luminosities using an inverted k-correction for the new distance. The standard γ-ray emission is extrapolated from GRB 130603B (Barthelmy et al. 2013), while the long lasting VHE γ-ray emission is extrapolated from *Fermi*-LAT observations of GRB 090510 (De Pasquale et al. 2010). In Sections 5.2.2 and 5.4, we consider three different X-ray counterparts and use three SGRBs with reasonable redshift constraints to quantify the typical fluxes given in Table 6, namely GRB 050509B for a SGRB without energy injection in the X-ray afterglow (Gehrels et al. 2005; Tunnicliffe et al. 2014), GRB 130603B for a long lived afterglow showing a clear signature of energy injection associated with a stable magnetar central engine (Fan, Wu & Wei 2013; de Ugarte Postigo et al. 2014; Fong et al. 2014), and GRB 080905A for an X-ray light curve with the signature of

Table 6. The typical expected emission from an on-axis compact binary merger at a distance of 200 Mpc for given observing latencies (– = no emission expected, ? = possible emission, refer to text for more details). We provide different predictions for the X-ray emission representing the range of different light curves observed from SGRBs (interpreted as different energy injection signatures; Rowlinson et al. 2013) and separate the SGRBs with bright and faint optical counterparts.

Wavelength	EM follow-up time				
	0 s	2 min	10 min	1 h	9 h
VHE γ-ray (>100 MeV, photon cm^{-2} s^{-1})	1.1×10^{1}	1.2×10^{-2}	$<1.7 \times 10^{-3}$	–	–
γ-ray (15–150 keV, photon cm^{-2} s^{-1})	3.2×10^{2}	?	?	–	–
X-ray – no energy injection (0.3–10 keV, erg cm^{-2} s^{-1})	–	7×10^{-12}	4×10^{-12}	2×10^{-12}	9×10^{-13}
X-ray – unstable magnetar (0.3–10 keV, erg cm^{-2} s^{-1})	–	3×10^{-9}	6×10^{-11}	5×10^{-13}	1×10^{-15}
X-ray – stable magnetar (0.3–10 keV, erg cm^{-2} s^{-1})	–	1×10^{-8}	6×10^{-9}	2×10^{-9}	8×10^{-11}
Optical – bright (R band, mag)	?	17.0	16.8	16.5	16.9
Optical – faint (R band, mag)	?	17.9	19.0	20.2	21.8
Radio (6.7 GHz, mJy)	?	?	?	?	11

Downloaded from https://academic.oup.com/mnras/article-abstract/459/1/121/2608842 by Universiteit van Amsterdam user on 03 July 2020

energy injection from a short-lived central engine, such as an unstable magnetar central engine (Rowlinson et al. 2010a, 2013). The radio fluxes given in Table 6 are extrapolated from GRB 130603B (Fong et al. 2014).

The optical magnitudes are determined at 200 Mpc using the standard formalism.[18] The optical afterglows are considered in Section 5.2.2; we typically observe very faint and rapidly fading optical afterglows to SGRBs and we represent these counterparts in Table 6 by extrapolating the optical counterpart to GRB 080905A (Rowlinson et al. 2010a). GRB 130603B had an unusually bright optical counterpart and we use this GRB to represent the bright optical afterglow in Table 6. Additionally, in Section 5.3, we consider the isotropic kilonova counterpart to GRB 130603B which would have an observed magnitude of $\sim$21 in the *J* band, but undetected in the *R* band to $\gtrsim$23.7, at a distance of 200 Mpc.

In the following sections, by combining the results from Tables 3–6 we discuss some possible observational opportunities and implications provided through a low-latency window.

6.2 Short duration GRBs

6.2.1 Probing the progenitor models of short GRBs

Coincident EM/GW observations of SGRBs can prove without doubt that BNS mergers are the progenitors behind these bursts. It is quite possible that one to two coincident events a year may be accessible at full aLIGO/AdV sensitivity using GRB satellites (Metzger & Berger 2012; Siellez, Boër & Gendre 2014; Regimbau et al. 2015). Such a verification could be provided by a wide FoV instrument such as *Fermi*. Low-latency follow-ups could also enable *multiwavelength* measurements of the prompt emission allowing the underlying central engine and emission mechanism to be probed (Elliott et al. 2014).

A particular obstacle faced by *Swift*-led observations of SGRBs is that the observed γ-ray emissions typically have observed durations shorter than 2 s. Therefore even a GW trigger with a latency as short as 10 s would not be sufficient to allow optical telescopes to recover emission during the prompt phase. However, a GW trigger sent out during the inspiral phase would allow multiwavelength telescopes be on target before the SGRB. Such a scenario could potentially provide a breakthrough in our understanding SGRB prompt emission physics.

In fact a number of foreseeable opportunities to study SGRB physics exist that could be plundered through low-latency follow-ups. Within the GRB theoretical framework, panchromatic emission during the prompt phase and early afterglow phase is predicted, including the emission from the prompt emission site through internal shocks (e.g. Meszaros & Rees 1993). Indeed, for long duration GRBs, panchromatic emission has been observed in a handful of *Swift* GRBs (e.g. Page et al. 2007; Zheng et al. 2012) thanks to their long durations or the existence of a precursor that triggered the *Swift* BAT. In particular, prompt optical flashes have been observed in a handful of long GRBs: e.g. the *Naked eye burst* GRB 080319B (Racusin et al. 2008), GRB 990123 (Akerlof et al. 1999), GRB 041219A (Vestrand et al. 2005), and GRB 130427B (Vestrand et al. 2014). However, so far no emission outside the γ-ray band has been detected during the prompt emission phase of SGRBs. Low-latency GW triggers 10s of seconds before merger could make this possible for the first time. As noted in Section 4.2, such observations will become more feasible once the error region is decreased through an expanded GW network in the latter part of the advanced GW detector era. For a particularly bright or close counterpart, the wide FoV and fast response of an instrument such as GWAC could prove to be highly valuable.

The high energy reach of *Fermi* has allowed access to photons with energies in access of 10 GeV in both long and SGRBs. The fact that *Fermi*-LAT discovered a photon of energy 31 GeV during the prompt phase of SGRB 090510 (Ackermann et al. 2010) is quite significant for low-latency follow-ups at VHE. In Table 6, we provide the expected VHE (>100 GeV) γ-ray flux and γ-ray flux for a putative SGRB at 200 Mpc coincident with a GW source. A low-latency trigger GW trigger would alert VHE and γ-ray detectors to search for prompt EM counterparts. In the γ-ray band the wide FoV of an instrument such as *Fermi* would be advantageous for such rapid follow-ups. At higher energies, instruments such as CTA could provide follow-ups in wide-field mode (Bartos et al. 2014); such observations would be very rich in high-energy photons and could provide valuable clues on the prompt emission mechanisms of SGRBs (Inoue et al. 2013; Bartos et al. 2014).

Additionally, we note that there are a small population of SGRBs that exhibit extended γ-ray emission for hundreds of seconds following the initial short burst (e.g. Norris & Bonnell 2006). This subpopulation of SGRBs are also believed to originate from compact binary mergers, and hence we might expect to observe this extended emission in some of the triggers even if the bright short-hard emission is missed by the γ-ray detectors due to the inadequate time for slew from the GW trigger. The possible response times provided for CTA in Table 3 suggest that VHE follow ups of these emissions are quite possible. Such observations could potentially unravel the exact nature of this extended activity (Inoue et al. 2013; Veres & Mészáros 2014).

6.2.2 Capturing the afterglow and late-time central engine activity of SGRBs

By comparing the expected X-ray counterparts given in Table 6 to the instruments described in Table 3, we show that existing X-ray instruments such as *Swift*-XRT or *Space-based multiband astronomical Variable Objects Monitor* (*SVOM*)-Microchannel X-ray Telescope (MXT) could detect the early X-ray afterglow for the SGRBs even without energy injection. Unfortunately, if the X-ray observations start with a latency longer than $\sim$10 min following the BNS merger, or they require a long time to tile out regions of the sky due to having a small FoV, we are likely to miss the X-ray counterparts for SGRBs without prolonged energy injection in their light curves (such as those described in Section 5.4).

We consider both bright and faint optical afterglows in Table 6 and note all of the optical instruments would be capable of observing the earliest onset (or the rise) of the optical afterglow assuming the 17th mag extrapolation based on a burst like GRB 130603B. However, GRB 130603B was unusually bright at early times, with a likely optical plateau phase, so the optical emission may have been contaminated with energy injection from the central engine (de Ugarte Postigo et al. 2014). Hence, these values are optimistic limits. Most SGRBs typically have a fainter counterpart, such as GRB 080905A, so will require deeper optical observations. The short optical reach and short exposure times of Pan-STARRS and ZTF suggest these instruments could be valuable in such

[18] The standard formula is $m - M = 5 \log D - 5$, with m the apparent magnitude, M is the absolute magnitude, and D is the luminosity distance in parsecs.

Downloaded from https://academic.oup.com/mnras/article-abstract/459/1/121/2608842 by Universiteit van Amsterdam user on 03 July 2020

endeavours. The larger FoV of ZTF would be more suited to searching the error regions from earlier GW triggers and could facilitate a coordinated search strategy with an instrument such as Pan-STARRS capable of deeper searches but more limited by FoV.

In the radio domain, there have been three detections of radio emission associated with SGRBs (GRB 050724, GRB 051221A, and GRB 130603B) as well as a forth case, GRB 120804A, due to host galaxy emission. In Table 6, we provide fluxes based on the radio counterpart of GRB 130603B. All of these detections have been at late times (>7 h) in the high-frequency domain (>4.9 GHz) with fluxes around the mJy level. These fluxes could be observed by instruments such as ASKAP or APERTIF. The peak in the radio afterglow would be expected to occur on typical time-scales of days–years. At low radio frequencies, we may also expect to observe the afterglow on months–years time-scales using facilities such as MWA and LOFAR although this emission has not been observed to date for a SGRB.

During the early afterglow phase, a short-lived backward propagating *reverse shock* component can occur once the shocked matter encounters the interstellar medium. This may dominate the optical and radio band under certain conditions, e.g. if the reverse shock region is more magnetized than the forward shock region (Zhang, Kobayashi & Mészáros 2003).

On short time-scales, an early radio flash (<1 d) originating from a reverse shock may be expected. Reverse shocks have been observed for a number of long GRBs, peaking a few hours after the GRB (e.g. GRB 130427A; Anderson et al. 2014; Perley et al. 2014) and may already have been observed in some SGRB radio afterglows (e.g. a radio excess was potentially observed at early times for GRB 130603B; Gompertz et al. 2015). Early radio observations, within the first hours of the BNS merger, capturing the rise of the reverse shock at different radio frequencies would allow detailed modelling of this mechanism and would be a valuable probe of the jet models, macrophysics within the jet and the surrounding environment of the GRB (as conducted for the long GRB 130427A by e.g. van der Horst et al. 2014). With its expected rapid triggering capabilities, ASKAP has the capability to detect an early reverse shock.

6.3 Kilonova

The peak frequency and brightness of a kilonova critically depend on the amount of ejected materials, and more importantly, the opacity of the ejecta. Early calculations adopted a relatively small opacity (e.g. Li & Paczyński 1998; Metzger et al. 2010; Bauswein, Goriely & Janka 2013), and predicted an optical transient with a peak flux about 1000 times of nova luminosity (and hence, the term 'kilonova' is coined) (Metzger et al. 2010). Barnes & Kasen (2013) pointed out that the existence of heavy elements, especially lanthanides, greatly increase the opacity, so that the kilonova signature would peak at a later time and in a softer frequency, typically in IR (see also Tanaka & Hotokezaka 2013).

The properties of the kilonova depend on the properties of the post-merger compact object. The calculations of Barnes & Kasen (2013) are relevant for the case of prompt formation of a black hole. If the merger product is a supramassive neutron star (sustained by rigid rotation for 100s of seconds or even longer, SMNS) or even a hypermassive neutron star (sustained by differential rotation for 100s of milliseconds, HMNS), neutrinos from the NS would raise the electron fraction and reduce the opacity, so that the kilonova signature is bluer and earlier (Metzger et al. 2015).

As discussed earlier, an observational candidate for a kilonova was claimed for SGRB 130603B (Berger et al. 2013; Tanvir et al. 2013) with one *Hubble Space Telescope* (*HST*) excess data point in the near-IR band 9 d after the SGRB. As shown in Section 5.1, this kilonova is equivalent to a *J*-band magnitude of 21 at 200 Mpc and an *R*-band magnitude of $\gtrsim$23.7. None of the optical telescopes given in Table 4 has near-IR capabilities and is not expected to detect an *R*-band counterpart at this observation time. Detailed modelling will be required to estimate the *R*-band fluxes and peak time-scales for these instruments (see the work by Barnes & Kasen 2013; Tanaka & Hotokezaka 2013). Besides this one case, two other candidates have been reported. One is an excess around 13.6 d in the *HST F814W* band following GRB 060614 (Yang et al. 2015); another is a significant optical rebrightening feature around 1 d following GRB 080503 (Perley et al. 2009; Gao et al. 2015). More data are needed to reveal the diverse kilonova phenomenology. A low-latency trigger would facilitate broad-band follow up observations to catch the kilonova signals, especially the early ones due to the small opacity in the ejecta. This will be a challenge due to the lack of sensitive instruments in the NIR band with FoVs large enough to survey the error regions (Bartos, Huard & Marka 2016). As discussed in the next section, an associated X-ray emission could be possible; this would allow a wide field instrument such as ISS-Lobster to narrow down the search area.

6.4 Magnetar formation

The X-ray plateaus attributed to a millisecond magnetar central engine are observed up to 100–10000 s after the bursts. The estimates in Table 6 show that if a stable magnetar is produced, GW triggers with a moderate latency could easily allow an X-ray instrument such as *Swift* to detect the plateau emission. However, should an unstable magnetar be produced, a GW trigger with a 40 s latency would be required enable an EM follow up within a few 100 s. Such observations of the plateau phase in combination with GW information could provide important clues of the NS equation of state (Lasky et al. 2014; Lü et al. 2015).

In addition to the X-ray plateaus, X-ray flares observed in the first few hundred seconds following short GRBs have also been interpreted as resulting from magnetic activity in a post-merger differentially rotating supramassive NS (Dai et al. 2006). Prompt follow ups of the GW signals from NS mergers would provide significant evidence for this formation channel of magnetars.

In the massive protomagnetar central engine model, the potentially wide-beamed magnetar wind is expected to produce a bright broad-band afterglow (Gao et al. 2013; Zhang 2013). This could result in an early afterglow in the optical (possibly as bright as 17th mag in *R* band) and X-ray bands (up to 10^{-8}–10^{-7} erg s^{-1} cm^{-2}) for a source at ∼300 Mpc (Zhang 2013).

The existence of a supramassive NS can also supply continuous heating to the ejecta which can, depending on the spin-down parameters of the neutron star, greatly enhance the kilonova signal (Yu et al. 2013; Metzger & Piro 2014). The detectability also depends on the observational geometry. For an on-axis binary merger, the signal may be fainter than the SGRB optical afterglow. However, for off-axis mergers, this would be the main UV/optical/IR signal from the event. The radio emission is also expected to peak earlier and brighter in this central engine model (e.g. Gao et al. 2013; Metzger & Bower 2014; Gompertz et al. 2015). These predicted optical and radio counterparts are potentially within the sensitivity and FoV capabilities of many of the optical and radio telescopes described in Tables 4 and 5.

Downloaded from https://academic.oup.com/mnras/article-abstract/459/1/121/2608842 by Universiteit van Amsterdam user on 03 July 2020

Additionally, recent suggestions that the observed prompt emission does not necessarily signal the start of the X-ray emission could have important consequences for low-latency follow-ups. Rezzolla & Kumar (2015) and Ciolfi & Siegel (2015) have postulated that the X-ray emission could start before the observed short hard spike emission of short GRBs. These models predict that X-ray emission from a protomagnetar could occur 100–1000 s prior to the prompt GRB.

It is clear that low-latency observations will play a major part in testing these models, but these will require more rapid triggering pipelines than those achievable by facilities such as *Swift* and *SVOM*-MXT (see Table 3). The employment of a wide FoV X-ray instrument with rapid pointing capabilities such as ISS-Lobster (Camp et al. 2013) would be very timely for the advanced GW detector era.

6.5 Fast radio bursts

The possibility of associations with FRBs and SGRBs and/or BNS mergers is still highly speculative.[19] Thornton et al. (2013) have suggested that the event rate of FRBs ($\sim 10^3$ gal^{-1} yr^{-1}) is inconsistent with GRBs and compact star mergers, but could be in agreement with soft gamma-ray repeaters or core-collapse supernovae. Totani (2013) argued that including the effects of cosmological time dilation and merger rate evolution would make the FRB event rate in agreement with the optimistic double NS merger event rate (Abadie et al. 2010). One caveat is that these models suggest an essentially isotropic emission of FRBs. However, due to the existence of the r-process ejecta launched before the coalescence, the FRB signal may not be able to escape the merger environment in most of the solid angles. Zhang (2014) acknowledged this and propose that the GRB- or merger-associated FRBs only account for a small fraction of the entire FRB population, and only those mergers whose jet direction coincides the observer's viewing direction (i.e. the short GRB direction) would be associated with FRBs. The majority of FRBs are attributed to those SMNSs whose delay time-scale to collapse into a black hole is much longer, and therefore not associated with GRBs or supernovae (Falcke & Rezzolla 2014). This is certainly an area where investments in GW low-latency trigger and prompt radio follow-up observations could provide significant scientific insight.

As discussed earlier, a particular obstacle for short duration events of order a few seconds is that even a latency as short as 10 s would not be sufficient to alert a γ-ray instrument in time to recover the prompt emission. This however can be circumvented in the radio band, by electronically steered radio arrays such as LOFAR, MWA, and, in the future, SKA-low. An instrument such as MWA could cover the entire GW error region in less than a minute of receiving a trigger. Although LOFAR typically has a smaller field of view than MWA (this is dependent upon observing configuration and frequency), it is also capable of tiling out large regions of the GW error box using multiple simultaneous pointing directions and can conduct commensal beam-formed observations to probe higher time resolutions. In addition, as MWA and LOFAR operate at low frequencies the signal will be delayed by propagation through the ionized intergalactic/interstellar media. Assuming a dispersion measure of 1000 pc cm^3, the delay could be of order 3 min at 150 MHz – sufficient time to point the telescope at the error region. With the voltage capture system on MWA and the transient buffer boards on LOFAR, in combination with the low-latency triggers and signal delay time, it will be possible for data to be obtained that can constrain emission from seconds to minutes prior to the merger. SKA-low is expected to have many of the capabilities of LOFAR and MWA but with a much higher sensitivity, making it the ideal future instrument for these triggers. For higher frequency instruments such as ASKAP and APERTIF, the delay would be significantly shorter – of order 8 s at 700 MHz – requiring much more rapid response times. Once on target, these radio telescopes would ideally continuously monitor the entire field for several hours as the different predicted FRB mechanisms cover a range of time-scales, both a few seconds prior to the merger and hours following it, and these observations would also be able to constrain the occurrence of other types of coherent radio emission.

[19] However, some models for coherent radio emission have been proposed the late stages of a compact binary inspiral phase or during their coalescence (e.g. Usov & Katz 2000).

7 DISCUSSION AND CONCLUSIONS

The first GW observation has provided a pathway to the highest energy density events in the Universe and transform our understanding of the behaviour of matter and space–time under the most extreme conditions. Coalescing systems of NSs are widely expected to be the progenitors of short GRBs. Early multiwavelength follow-up observations of these sources would allow one to probe and unravel the mechanisms behind these events beyond the GW regime; the potential for breakthrough science is without doubt.

In this study we have simulated the expected localization error regions corresponding to different times before the merger of a coalescing system of NSs. To examine the most probable low-latency EM observations we have considered the benefit provided by (a) larger networks of GW detectors, corresponding with improved localization; (b) improved GW triggering latencies for sending out GW triggers.

The tables shown in Figs 5 and 6 illustrate some of the multi-messenger observations that could be achieved through low-latency GW triggers assuming a detection 40 s before merger. We note here that these tables may well be riddled with caveats due to the different operating scenarios and evolution of the different wavelength instruments. Furthermore, it would require very detailed modelling to predict exact fluxes of the different EM emission mechanisms; well beyond the scope of this work. The goal of this study is to highlight the type of breakthrough science that could be realized through the low-latency domain and, using a wide selection of EM instruments with agreements in place with aLIGO/AdV for follow-up observations, determine the most likely avenues for success.

Fig. 5 presents a conservative scenario; that of a LHV network corresponding with a 1000 deg^2 error region (assuming the 50 per cent case provided in Table 2) and a 40 s GW triggering latency to send out the alert. At low-frequency radio and both high- and low-energy γ-ray, the large FoV and fast response potential show that post-prompt ($>$5 s) breakthrough observations could be realized.

In the optical, even for Pan-STARRS and ZTF, both large FoV instrument with fast responses, to cover the 1000 deg^2 error region with an exposure times of 30 s would require $>$(4000; 600) s, respectively. For longer latency follow-ups, optical instruments available in the latter stages of the aLIGO/AdV era include BlackGEM which has a 40 deg^2 FoV and a depth of 22 mag and a possible future configuration of GOTO, which could employ a 40–50 deg^2 instantaneous FoV and sensitivity to 20–21.5 mag (Steeghs & Galloway, personal communication).

Downloaded from https://academic.oup.com/mnras/article-abstract/459/1/121/2608842 by Universiteit van Amsterdam user on 03 July 2020

SIGNAL TYPE	TARGET	TIME RANGE (s)	Gamma		X-ray	Optical/IR	Radio	
			High (> 10 MeV)	Low (< 10 MeV)			High (> 1 GHz)	Low (< 1 GHz)
Jet Related	SGRB Prompt	0-5	✓	✓	?	?		
	SGRB Afterglow	10 ->	✓		✓	✓	✓	?
	Reverse Shock	60-10000	?	?	?	?	✓	?
Isotropic Ejecta Related	Kilonova	1000 ->			?	✓		
	Ejecta Afterglow	10000 ->			?	?	?	?
Other Signals	Magnetar Wind Dissipation	1-1000	?	✓	✓	?	?	?
	FRB (early)	-5 -10					?	?
	FRB (late)	10-10000					?	?

	Response fast enough FoV within range		Fast response FoV too small	✓	Observed
	Response too slow FoV within range		Response too slow + FoV too small	?	Predicted

Figure 5. Some of the multimessenger observations that could be achieved through low-latency GW triggers. All scenarios assume a detection 40 s before merger by an LHV network – corresponding with a 1000 deg^2 error region – and a 40 s GW triggering latency to send out the GW trigger. The signals are grouped by into jetted, isotropic, or unknown; the approximate emission time ranges around merger are also given. As shown by the legend, the ticks indicate the EM observations with observational support; the question marks indicate those that have been proposed through theoretical models. All possible observations in the table are given a colour code; good news is given by dark shaded cells that indicate there are EM instruments available in the band with sufficiently fast responses, exposure times and FoVs to cover or tile the GW error box within the emission time range; at the other extreme, light shaded cells indicate that EM follow-up observations will be quite challenging. Between these two extremes there is scope for improvement; for example ToOs could potentially be speeded up or wider FoV instruments could come on line.

SIGNAL TYPE	TARGET	TIME RANGE (s)	Gamma		X-ray	Optical/IR	Radio	
			High (> 10 MeV)	Low (< 10 MeV)			High (> 1 GHz)	Low (< 1 GHz)
Jet Related	SGRB Prompt	0-5	✓	✓	?	?		
	SGRB Afterglow	10s->	✓		✓	✓	✓	?
	Reverse Shock	60-10000	?	?	?	?	✓	?
Isotropic Ejecta Related	Kilonova	1000 ->			?	✓		
	Ejecta Afterglow	10000 ->			?	?	?	?
Other Signals	Magnetar Wind Dissipation	1-1000	?	✓	✓	?	?	?
	FRB (early)	-5 -10					?	?
	FRB (late)	10-10000					?	?

Figure 6. As for Fig. 5 but assuming an expanded LHVJIA network – corresponding with an 182 deg^2 error region, and a 1 s GW triggering latency to send out the GW trigger. This figure shows what could be achieved by EM instruments given a ∼40 s head start to get on-source.

To catch the early prompt stage, assuming a 40 s GW triggering latency, even instruments with a large FoV will be challenged; this scenario certainly provides motivation for speeding up the trigger pipelines of both the GW observatories as well as the high-energy satellites. We note that for the low-frequency radio, one bonus in regards to EM follow-ups is that the dispersion of coherent radio signals can introduce a significant delay of up to minutes (as discussed in Section 6.5); as the existence of early time counterparts to coalescing BNSs in the radio band are still highly speculative, we have taken a conservative approach and neglected this effect, assuming only the physical time in our estimates.

Downloaded from https://academic.oup.com/mnras/article-abstract/459/1/121/2608842 by Universiteit van Amsterdam user on 03 July 2020

A more optimistic scenario is presented in Fig. 6 which shows how breakthrough science can be achieved with an almost instantaneous 1 s GW triggering latency and a fully expanded advanced detector network, LHVJIA. For the 182 deg^2 error region the post-prompt (>5 s) situation is much more optimistic in the optical and high-frequency radio bands due to the FoVs of radio instruments with responses <min and wide FoV telescopes such as ZTF that could survey this error region in around 2 min. In the X-ray, small FoV instruments such as *Swift* are hindered by the large GW error region. Although considerable efforts have been undertaken to remedy this situation through the use a requirement for reconstructed sky locations to overlap with nearby galaxies (Evans et al. 2012), this coupled with the slow response of high-energy satellites presents a significant bottleneck in a band for which many of the post-merger EM emissions are known to exist. It emphasizes the importance to have a wide FoV X-ray instrument capable of rapid pointing; one potential instrument that could remedy the situation is the NASA proposed 30 deg^2 FoV soft X-ray instrument ISS-Lobster (Camp et al. 2013).

For prompt (<5 s) observations the wide FoV of *Fermi* means this instrument could provide a coincident observation with a GW trigger – this scenario is considered in the low gamma-ray (<10 MeV) region of Figs 5 and 6. However, we note the slow response of other satellites operating at the low γ will hinder prompt follow-ups. If such a low GW triggering latency could be achieved and instruments such as *Swift*/*Fermi* could employ fast triggering pipelines, and a wide FoV X-ray instrument could be employed, low-latency EM follow-ups with a full GW global network would enjoy almost complete coverage for the models we have considered.

We note that the scenarios we have outlined in Figs 5 and 6 assume the GW error regions 40 s before merger; this choice was to provide the EM facilities with the maximum time for response. However, as shown in Table 2, closer to the merger both the error regions contract and the percentage of detections sources increases. For sources detected early in the inspiraling stage, subsequent alerts would most likely be sent out as the error box decreases in size; this suggests that a coordinated observational and alerting strategy involving both the GW network and both wide and narrower FoV instruments would be optimal procedure for maximizing GW detections.

Our results support the argument that much breakthrough science can be achieved through a fast response. This has been evidenced in the post-*Swift* era with prompt follow-up of GRB triggers producing such unexpected phenomena as flares, plateaus, optical flashes, and reverse shocks. History therefore suggests that the lasting legacy from the era of prompt multiwavelength GW follow-ups will undoubtedly be provided by the unexpected surprises we encounter.

ACKNOWLEDGEMENTS

Much of the analysis and discussion in this paper would not have been possible without the valuable input from members of the various EM facilities. In particularly we would like to thank David Kaplan, Shami Chatterjee, and Lisa Harvey-Smith (ASKAP), Dipankar Bhattacharya (Astrosat/CZTI), Imre Bartos (Columbia U), Paul O'Brien, Jim Hinton, and Gavin Rowell (CTA), Peter Jonker (LOFAR), Julie McEnery and Valerie Connaughton (*Fermi*), Weiming Yuan, Chao Wu, and Jianyan Wei (NAOC), Fang Yuan (SkyMapper), Duncan Galloway and Danny Steeghs (GOTO), and David Coward (Zadko). We are particularly grateful to Julie McEnery (NASA/GSFC) who contributed some valuable suggestions for Section 4.1 and to Paul Laskey (Monash University) who provided some useful comments to improve the paper. We acknowledge support from WA's Pawsey Supercomputing Center. EJH acknowledges support from a UWA Research Fellowship. LW is supported by the Australian Research Council. BZ acknowledges NASA NNX14AF85G and NNX15AK85G for partial support. The authors gratefully thank Leo Singer, the assigned reviewer for the LIGO Scientific Collaboration, for conducting a thorough review of the manuscript which included a number of insightful suggestions. Finally, the authors thank the anonymous referee whose valued comments have vastly improved the structure of the paper.

REFERENCES

Aasi J. et al., 2013, Prospects for Localization of Gravitational Wave Transients by the Advanced LIGO and Advanced Virgo Observatories
Aasi J. et al., 2015, Classical Quantum Gravity, 32, 074001
Abadie J. et al., 2010, Classical Quantum Gravity, 27, 173001
Abadie J. et al., 2012, A&A, 539, A124
Abadie J. et al., 2012, A&A, 541, A155
Abbott B. P. et al., 2016a, Phys. Rev. Lett., 116, 061102
Abbott B. P. et al., 2016b, ApJ, 818, L22
Acernese F. et al., 2015, Classical Quantum Gravity, 32, 024001
Ackermann M. et al., 2010, ApJ, 716, 1178
Aharonian F. et al., 2009, A&A, 495, 505
Akerlof C. et al., 1999, Nature, 398, 400
Anderson G. E. et al., 2014, MNRAS, 440, 2059
Aso Y. et al., 2013, Phys. Rev. D, 88, 043007
Atwood W. B. et al., 2009, ApJ, 697, 1071
Barnes J., Kasen D., 2013, ApJ, 775, 18
Barthelmy S. D. et al., 2005a, Nature, 438, 994
Barthelmy S. D. et al., 2005b, ApJ, 635, L133
Barthelmy S. D. et al., 2013, GRB Coordinates Network, 14741, 1
Bartos I. et al., 2014, MNRAS, 443, 738
Bartos I., Huard T. L., Marka S., 2016, ApJ, 816, 61
Bauswein A., Goriely S., Janka H.-T., 2013, ApJ, 773, 78
Bellm E., 2014, in Wozniak P. R., Graham M. J., Mahabal A. A., Seaman R., eds, The Third Hot-wiring the Transient Universe Workshop: The Zwicky Transient Facility, p. 27, preprint (arXiv:1410.8185)
Berger E., 2011, New. Astron. Rev., 55, 1
Berger E., 2014, ARA&A, 52, 43
Berger E. et al., 2005, Nature, 438, 988
Berger E., Fong W., Chornock R., 2013, ApJ, 774, L23
Bloom J. S., Frail D. A., Sari R., 2001, AJ, 121, 2879
Bloom J. S. et al., 2006, ApJ, 638, 354
Burrows D. N. et al., 2006, ApJ, 653, 468
Buskulic D., Virgo Collaboration, LIGO Scientific Collaboration, 2010, Classical Quantum Gravity, 27, 194013
Camp J. et al., 2013, Exp. Astron., 36, 505
Campana S. et al., 2006, Nature, 442, 1008
Cannon K. et al., 2012, ApJ, 748, 136
Centrella J., Nissanke S., Williams R., 2012, in Griffin E., Hanisch R., Seaman R., eds, Proc. IAU Symp. 285, New Horizons in Time-Domain Astronomy. Cambridge Univ. Press, Cambridge, p. 191
Chu Q., Wen L., Blair D., 2012, J. Phys.: Conf. Ser., 363, 012023
Chung S. K., Wen L., Blair D., Cannon K., Datta A., 2010, Classical Quantum Gravity, 27, 135009
Ciolfi R., Siegel D. M., 2015, ApJ, 798, L36
Coward D. M. et al., 2010, Publ. Astron. Soc. Aust., 27, 331
Coward D. M. et al., 2012, MNRAS, 425, 2668
Coward D. M., Branchesi M., Howell E. J., Lasky P. D., Böer M., 2014, MNRAS, 445, 3575
Cowperthwaite P. S., Berger E., 2015, ApJ, 814, 25
Cramer H., 1946, Mathematical Methods of Statistics. Princeton Univ. Press, Princeton, NJ
Dai Z. G., Lu T., 1998, A&A, 333, L87
Dai Z. G., Wang X. Y., Wu X. F., Zhang B., 2006, Science, 311, 1127
De Pasquale M. et al., 2010, ApJ, 709, L146

Downloaded from https://academic.oup.com/mnras/article-abstract/459/1/121/2608842 by Universiteit van Amsterdam user on 03 July 2020

Dessart L., Ott C. D., Burrows A., Rosswog S., Livne E., 2009, ApJ, 690, 1681
de Ugarte Postigo A. et al., 2014, A&A, 563, A62
Doro M. et al., 2013, Astropart. Phys., 43, 189
Dubus G. et al., 2013, Astropart. Phys., 43, 317
Eichler D., Livio M., Piran T., Schramm D. N., 1989, Nature, 340, 126
Elliott J. et al., 2014, A&A, 562, A100
Evans P. A. et al., 2012, ApJS, 203, 28
Fairhurst S., 2009, New J. Phys., 11, 123006
Fairhurst S., 2011, Classical Quantum Gravity, 28, 105021
Falcke H., Rezzolla L., 2014, A&A, 562, A137
Fan Y.-Z., Xu D., 2006, MNRAS, 372, L19
Fan Y.-Z., Wu X.-F., Wei D.-M., 2013, Phys. Rev. D, 88, 067304
Fan X., Messenger C., Heng I. S., 2014, A Bayesian approach to multi-messenger astronomy: Identification of gravitational-wave host galaxies
Fernández R., Metzger B. D., 2013, MNRAS, 435, 502
Finn L. S., 1992, Phys. Rev. D, 46, 5236
Fong W. et al., 2014, ApJ, 780, 118
Funk S., Hinton J. A., CTA Consortium, 2013, Astropart. Phys., 43, 348
Gao W.-H., Fan Y.-Z., 2006, Chin. J. Astron. Astrophys., 6, 513
Gao H., Ding X., Wu X.-F., Zhang B., Dai Z.-G., 2013, ApJ, 771, 86
Gao H., Ding X., Wu X.-F., Dai Z.-G., Zhang B., 2015, ApJ, 807, 163
Gehrels N. et al., 2004, ApJ, 611, 1005
Gehrels N. et al., 2005, Nature, 437, 851
Ghosh S., Nelemans G., 2015, in Sopuerta C. F., ed., Astrophys. Space Sci. Proc. Vol. 40, Gravitational Wave Astrophysics. Springer International Publishing, Switzerland, p. 51
Giacomazzo B., Perna R., 2013, ApJ, 771, L26
Gompertz B. P., van der Horst A. J., O'Brien P. T., Wynn G. A., Wiersema K., 2015, MNRAS, 448, 629
Götz D. et al., 2014, Proc. SPIE, 9144, 914423
Hodapp K. W., Siegmund W. A., Kaiser N., Chambers K. C., Laux U., Morgan J., Mannery E., 2004, Proc. SPIE, 5489, 667
Hooper S., Chung S. K., Luan J., Blair D., Chen Y., Wen L., 2012, Phys. Rev. D, 86, 024012
Hotokezaka K., Kiuchi K., Kyutoku K., Muranushi T., Sekiguchi Y.-i., Shibata M., Taniguchi K., 2013, Phys. Rev. D, 88, 044026
Howell E. J. et al., 2015, Publ. Astron. Soc. Aust., 32, e046
Inoue S. et al., 2013, Astropart. Phys., 43, 252
Jaranowski P., Królak A., Schutz B. F., 1998, Phys. Rev. D, 58, 063001
Johnston S. et al., 2007, Publ. Astron. Soc. Aust., 24, 174
Kanner J., Camp J., Racusin J., Gehrels N., White D., 2012, ApJ, 759, 22
Keller S. C. et al., 2007, Publ. Astron. Soc. Aust., 24, 1
Klimenko S. et al., 2011, Phys. Rev. D, 83, 102001
Klotz A., Boer M., Atteia J.-L., Gendre B., Le Borgne J.-F., Frappa E., Vachier F., Berthier J., 2013, Messenger, 151, 6
Kulkarni S. R., 2005, preprint (arXiv:Astrophys. e-prints)
Lasky P. D., Haskell B., Ravi V., Howell E. J., Coward D. M., 2014, Phys. Rev. D, 89, 047302
Lee W. H., Ramirez-Ruiz E., López-Cámara D., 2009, ApJ, 699, L93
Lennarz D., Chadwick P. M., Domainko W., Parsons R. D., Rowell G., Tam P. H. T., for the H. E. S. S. Collaboration, 2013, preprint (arXiv:1307.6897)
Li L.-X., Paczyński B., 1998, ApJ, 507, L59
LIGO Scientific Collaboration, 2009, Advanced LIGO Anticipated Sensitivity Curves, LIGO Document T-0900288-v2
Liu Y., Du Z., Chung S. K., Hooper S., Blair D., Wen L., 2012, Classical Quantum Gravity, 29, 235018
Lorimer D. R., Karastergiou A., McLaughlin M. A., Johnston S., 2013, MNRAS, 436, L5
Lü H.-J., Zhang B., Lei W.-H., Li Y., Lasky P. D., 2015, ApJ, 805, 89
Luan J., Hooper S., Wen L., Chen Y., 2012, Phys. Rev. D, 85, 102002
Manzotti A., Dietz A., 2012, preprint (arXiv:e-prints)
Meegan C. et al., 2009, ApJ, 702, 791
Meszaros P., Rees M. J., 1993, ApJ, 405, 278
Metzger B. D., Berger E., 2012, ApJ, 746, 48
Metzger B. D., Bower G. C., 2014, MNRAS, 437, 1821
Metzger B. D., Piro A. L., 2014, MNRAS, 439, 3916
Metzger B. D., Quataert E., Thompson T. A., 2008, MNRAS, 385, 1455
Metzger B. D. et al., 2010, MNRAS, 406, 2650
Metzger B. D., Giannios D., Thompson T. A., Bucciantini N., Quataert E., 2011, MNRAS, 413, 2031
Metzger B. D., Bauswein A., Goriely S., Kasen D., 2015, MNRAS, 446, 1115
Murphy T. et al., 2013, Publ. Astron. Soc. Aust., 30, 6
Nakar E., Piran T., 2011, Nature, 478, 82
Narayan R., Paczynski B., Piran T., 1992, ApJ, 395, L83
Nissanke S., Holz D. E., Hughes S. A., Dalal N., Sievers J. L., 2010, ApJ, 725, 496
Nissanke S., Sievers J., Dalal N., Holz D., 2011, ApJ, 739, 99
Nissanke S., Kasliwal M., Georgieva A., 2013, ApJ, 767, 124
Norris J. P., Bonnell J. T., 2006, ApJ, 643, 266
Oosterloo T., Verheijen M., van Cappellen W., 2010, in ISKAF2010 Science Meeting The Latest on Apertif. p. 43
Özel F., Psaltis D., Narayan R., Villarreal A. S., 2012, ApJ, 757, 55
Paczynski B., 1986, ApJ, 308, L43
Paczýnski B., 1991, Acta Astron., 41, 257
Page K. L. et al., 2007, ApJ, 663, 1125
Paul J., Wei J., Basa S., Zhang S.-N., 2011, Comptes Rendus Phys., 12, 298
Perley D. A. et al., 2009, AJ, 138, 1690
Perley D. A. et al., 2014, ApJ, 781, 37
Piran T., Nakar E., Rosswog S., 2013, MNRAS, 430, 2121
Prasad P., Wijnholds S. J., Huizinga F., Wijers R. A. M. J., 2014, A&A, 568, A48
Punturo M., 2012, Note vir-0128a-12, Advanced Virgo Technical Design Report. The Virgo Collaboration
Racusin J. L. et al., 2008, Nature, 455, 183
Ravi V., Lasky P. D., 2014, MNRAS, 441, 2433
Regimbau T., Siellez K., Meacher D., Gendre B., Boër M., 2015, ApJ, 799, 69
Rezzolla L., Kumar P., 2015, ApJ, 802, 95
Rezzolla L., Giacomazzo B., Baiotti L., Granot J., Kouveliotou C., Aloy M. A., 2011, ApJ, 732, L6
Rosswog S., Piran T., Nakar E., 2013, MNRAS, 430, 2585
Rowlinson A. et al., 2010a, MNRAS, 408, 383
Rowlinson A. et al., 2010b, MNRAS, 409, 531
Rowlinson A., O'Brien P. T., Metzger B. D., Tanvir N. R., Levan A. J., 2013, MNRAS, 430, 1061
Schutz B. F., 2011, Classical Quantum Gravity, 28, 125023
Shawhan P. S., 2012, Proc. SPIE, 8448, 84480Q
Shibata M., Taniguchi K., Okawa H., Buonanno A., 2014, Phys. Rev. D, 89, 084005
Siellez K., Boër M., Gendre B., 2014, MNRAS, 437, 649
Singer L. P., 2015, PhD thesis, California Institute of Technology
Singer L. P. et al., 2013, ApJ, 776, L34
Singer L. P. et al., 2014, ApJ, 795, 105
Singer L. P. et al., 2015, ApJ, 806, 52
Smith R. M. et al., 2014, Proc. SPIE, 9147, 79
Somiya K., 2012, Classical Quantum Gravity, 29, 124007
Staley T. D. et al., 2013, MNRAS, 428, 3114
Tanaka M., Hotokezaka K., 2013, ApJ, 775, 113
Tanvir N. R., Levan A. J., Fruchter A. S., Hjorth J., Hounsell R. A., Wiersema K., Tunnicliffe R. L., 2013, Nature, 500, 547
Thornton D. et al., 2013, Science, 341, 53
Tingay S. J. et al., 2013, Publ. Astron. Soc. Aust., 30, 7
Totani T., 2013, PASJ, 65, L12
Tremblay S. E. et al., 2015, Publ. Astron. Soc. Aust., 32, 5
Troja E. et al., 2007, ApJ, 665, 599
Tunnicliffe R. L. et al., 2014, MNRAS, 437, 1495
Usov V. V., Katz J. I., 2000, A&A, 364, 655
van der Horst A. J. et al., 2014, MNRAS, 444, 3151
van Haarlem M. P. et al., 2013, A&A, 556, A2
Veres P., Mészáros P., 2014, ApJ, 787, 168
Verheijen M. A. W., Oosterloo T. A., van Cappellen W. A., Bakker L., Ivashina M. V., van der Hulst J. M., 2008, in Minchin R., Momjian E.,

Downloaded from https://academic.oup.com/mnras/article-abstract/459/1/121/2608842 by Universiteit van Amsterdam user on 03 July 2020

eds, AIP Conf. Proc. Vol. 1035, The Evolution of Galaxies Through the Neutral Hydrogen Window. Am. Inst. Phys., New York, p. 265
Vestrand W. T. et al., 2005, Nature, 435, 178
Vestrand W. T. et al., 2014, Science, 343, 38
Vitale S., Zanolin M., 2011, Phys. Rev. D, 84, 104020
Wen L., Chen Y., 2010, Phys. Rev. D, 81, 082001
Wen L., Fan X., Chen Y., 2008, J. Phys. Conf. Ser., 122, 012038
Yang B. et al., 2015, Nat. Commun., 6, 7323
Yu Y., Huang Y.-F., 2007, Chin. J. Astron. Astrophys., 7, 669
Yu Y.-W., Zhang B., Gao H., 2013, ApJ, 776, L40
Zanolin M., Vitale S., Makris N., 2010, Phys. Rev. D, 81, 124048
Zhang B., 2013, ApJ, 763, L22
Zhang B., 2014, ApJ, 780, L21
Zhang B., Mészáros P., 2001, ApJ, 552, L35
Zhang B., Kobayashi S., Mészáros P., 2003, ApJ, 595, 950
Zheng W. et al., 2012, ApJ, 751, 90

This paper has been typeset from a TEX/LATEX file prepared by the author.

Downloaded from https://academic.oup.com/mnras/article-abstract/459/1/121/2608842 by Universiteit van Amsterdam user on 03 July 2020